THESIS FOR THE DEGREE OF DOCTOR OF PHILOSOPHY

LASER PHOTODETACHMENT OF NEGATIVE IONS

Fundamental Research and Applications

PONTUS ANDERSSON

Department of Physics
University of Gothenburg
Gothenburg, Sweden 2009

UNIVERSITY OF GOTHENBURG

PONTUS ANDERSSON
April 24, 2009

Department of Physics
University of Gothenburg
SE-412 96 Gothenburg, Sweden
Phone: +46 (0)31–772 1000

Contact information:
Pontus Andersson
Department of Physics
University of Gothenburg

SE-412 96 Gothenburg, Sweden

Phone: +46 (0)31–772 3297
Fax: +46 (0)31–772 3663
Email: pontus.andersson@physics.gu.se

To my family.

”I love you guys”
- Eric Cartman
South Park, season 2, episode 5

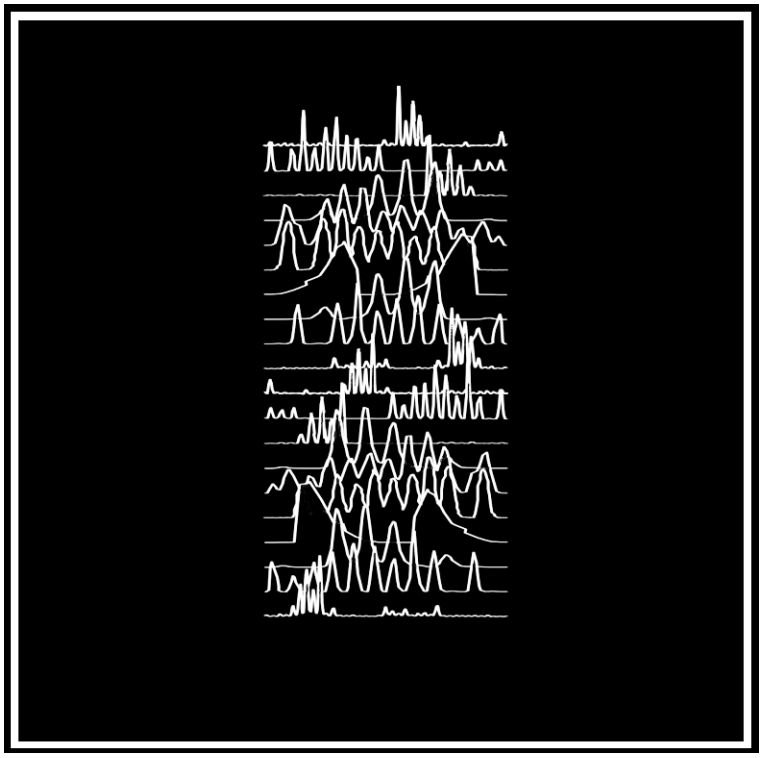

Abstract

Photodetachment studies of atomic and molecular negative ions in the gas phase are presented. Negative ions are loosely bound quantum systems whose existence is strongly dependent on the correlations between the electrons. This makes sophisticated calculations of the structure and dynamics for these systems complex and experimental data are needed for verification. Negative ions are also important in applications such as plasma etching and atmospheric studies. One of the most important applications for negative ions is as the state of matter for injection in tandem accelerators used in Accelerator Mass Spectrometry (AMS), the most sensitive method for ultra trace isotope analysis. Using negative ions in the injection stage provides isobar suppression in cases where the contaminating isobar does not form stable negative ions. Several experiments on laser interaction with a beam of mass-selected negative ions are presented. The objective for these studies can be divided into three subgroups: structure studies, dynamic studies, and proof-of-principle experiments for applications of negative ions. In the first group, the value for the electron affinity and the fine structure splitting of phosphorus is refined. The value of the electron affinity of tungsten is improved and the origin of the photodetachment signal below threshold is discussed. Resonant structure in the cross section and the electron affinity of cerium is treated. Finally, a predicted excited state in platinum is observed experimentally for the first time. The second group consists of the lifetime measurements of metastable excited states for tellurium, selenium and silicon. These measurements were made at the magnetic heavy ion storage ring CRYRING at Manne Siegbahn Laboratories in Stockholm. The third and last group are proof-of-principle experiments of isobar and neighboring isotope suppression by laser interaction. Suppression of up to four orders of magnitude is reached and the implementation into mass spectrometric systems are discussed.

Keywords: Negative Ions, Laser Spectroscopy, Photodetachment, Electron Affinity, Mass Spectrometry, Radiative Lifetimes, Storage Rings.

List of Appended Papers

This thesis is a summary of seven published articles and three manuscripts. References to the papers will be made using Roman numbers.

I. P Andersson, A O Lindahl, C Alfredsson, L Rogström, C Diehl, D J Pegg and D Hanstorp. **The electron affinity of phosphorus.** J. Phys. B: At. Mol. Opt. Phys. **40** 40974107 (2007)

II. A O Lindahl, P Andersson, C Diehl and D Hanstorp. **The electron affinity of tungsten.** In manuscript.

III. C W Walter, N D Gibson, P Andersson, C M Janczak, K A Starr, A P Snedden, and R L Field III. **Infrared photodetachment of Ce^-: Threshold spectroscopy and resonance structure.** Physical Review A **76**, 052702 (2007)

IV. P Andersson, A O Lindahl, D Hanstorp and D J Pegg. **Observation of the $^2S_{1/2}$ metastable state in Pt^-.** Physical Review A **79**, 022502 (2009)

V. A Ellmann, P Schef, P Lundin, P Royen, S Mannervik, K Fritioff, P Andersson, D Hanstorp, C F Fischer, F Österdahl, D J Pegg, N D Gibson, H Danared and A Källberg . **Radiative lifetime of a bound excited state of Te^-.** Physical Review Letters. **92** (25)(2004)

VI. P Andersson, K Fritioff, J Sandström, G Collins, D Hanstorp, A Ellmann, P Schef, P Lundin, S Mannervik, P Royen, K C Froese Fischer, F Österdahl, D Rostohar, D J Pegg, N D Gibson, H Danared, and A Källberg. **Radiative lifetimes of metastable states of negative ions.** Physical Review A **73**, 032705 (2006)

VII. J Sandström, P Andersson, K Fritioff, D Hanstorp, R Thomas, D J Pegg and K Wendt **Laser photodetachment mass spectrometry.** Nuclear Instruments and Methods in Physics Research B **217** 513520 (2004)

VIII. P Andersson, J Sandström, D Hanstorp, N D Gibson, K Wendt, D J Pegg and R D Thomas. **Selective detection of ^{13}C by laser photodetachment mass spectrometry.** Nuclear Instruments and Methods in Physics Research B **266** 36673673 (2008)

IX. P Klason, P Andersson, A O Lindahl, D Hanstorp, C Diehl, and O Forstner **A lower limit for ground state photodetachment of hafnium and tungsten penta-fluorides** In manuscript.

X. P Andersson, Y Liu and C C Havener **Improved method for determination of the suppression of isobars in a gas-filled rf-quadrupole ion-guide.** In manuscript.

The following publications have not been included in the thesis since they are focused on detachment by electron collision and not on laser photodetachment:

- A Lindahl, P Andersson, G F Collins *et al.* Experimental investigation of electron impact on Si_2^-. Physical review A. **77** (2) s. 022710 (2008).
- K Fritioff, J Sandström, P Andersson *et al.* Observation of an excited C_4^{2-} ion. Journal of Physics B-Atomic Molecular and Optical Physics. **37** (11) s. 2241-2246 (2004).
- K Fritioff, J Sandström, P Andersson *et al.* Single and double detachment from H^-. Physical Review A. **69** (4)(2004).

The following publication have not been included in the thesis since inner shell photodetachment is not within the scope of the thesis:

- R C Bilodeau, N D Gibson, P Andersson *et al.* High-charge-state formation following inner-shell photodetachment from S^-. Physical Review A. **72** s. 050701 (2005).

Table 1: Energies in this thesis are mainly given in the units of cm^{-1} or eV. For the reader who is interested in comparing these units, a conversion table is provided here.

eV	cm^{-1}	Hz
1	$8.065545 \cdot 10^{3}$	$2.417989 \cdot 10^{14}$
$1.239842 \cdot 10^{-4}$	1	$2.997925 \cdot 10^{10}$
$4.135667 \cdot 10^{-15}$	$3.335641 \cdot 10^{-11}$	1

My contribution to the articles included in this thesis is as follows:
I took part in performing and preparing the experiments for all papers.
For paper **III**, I was only participating in parts of the data collection.
I was participating in rebuilding the experimental setup used in paper **III**.
I was responsible for the complete data analysis in papers **I, IV** and **VIII** and partially responsible for the analysis of data for papers **II, V, VI, VII** and **IX**
I wrote the first versions of papers **IV, VI** and **X**.

Contents

1 Introduction

A negative ion is an atom or a molecule to which an extra electron has been attached, giving the whole system a net negative charge. Such systems are more fragile and more difficult to observe than their positive counterparts and were therefore not explored with the same thoroughness in the early days of quantum physics. Today the structure of most negative ions is well known, but there still exist gaps in the data, especially in the heavier part of the periodic system. The aim of this thesis is to contribute to the knowledge of fundamental negative ion properties, as well as to explore applications by means of the knowledge gained through the years since Thomson's first discovery of negatively charged atoms and molecules.

1.1 A Brief History

Sir Joseph John Thomson discovered the electron in 1897 when he was investigating cathode rays. Later he continued his work by refining the early mass spectrometry methods of W. Wien. By separating particles by their ratio of charge to mass and allowing the particles to strike a photographic plate, he was able to distinguish, in his own words [1], between:

I. Positively electrified atoms with one charge.

II. Positively electrified molecules with one charge.

III. Positively electrified atoms with multiple charges.

IV. *Negatively electrified atoms.*

V. *Negatively electrified molecules.*

Although Thomson was mainly concerned with positive ions, this is to my knowledge the first time negative ions in the gas phase were mentioned in the literature.

Forty years later, in 1938, Massey collected almost everything that was then known about negative ions at that time in the first edition of his book *Negative Ions* [2]. The deviation from the Planck curve characteristic of a black-body in the continuous solar spectrum was ascribed by Wildt to the atomic negative hydrogen ion in 1939 [3]. Hydrogen was known to be the main constituent of the sun and free electrons are readily made by the ionization of metals such as Na, Mg, Ca and Fe. The formation of negative hydrogen ions is therefore very plausible. Wildt then suggested that the absorption found in the infrared part of the sun's black-body radiation spectrum was caused by photodetachment of negative hydrogen ions in the sun's photosphere. Subsequent calculations [4] supported this, but a precise measurement of the binding energy for the negative hydrogen ion was missing. This spurred experimental investigations, and different techniques for negative ion beam production were developed. In 1953 W. L. Fite tested five different sources to find the best means of negative ion beam production [5]. He settled for the dc glow discharge source. Fite's results allowed him and M. L. Branscomb to perform the first photodetachment experiment in 1953 [6]. Two years later Branscomb and Smith measured the photodetachment cross sections for H^- and D^- [7]. A second updated edition of Massey's book came in 1950 and a third edition was published in 1976 [8]. In 1965, B M Smirnov summed up the current knowledge on atomic negative ions in an extensive review article [9]. Systematic studies of the binding energies for many of the atoms in the periodic system were started in 1970 [10–14] and reviewed in 1975 by H. Hotop and W. C. Lineberger [15]. This review of negative ion structure data has since been updated twice, with the latest edition in 1999 [16]. Other authors have recently written extensive reviews of the field [17] as well as specific reviews treating different aspects of the negative ions such as photodetachment experiments using atom and ion detection [18] and resonances in photodetachment cross sections [19].

1.2 Interest in Fundamental Properties of Negative Ions

Negative ions are fascinating quantum systems with physical properties that play important roles in many different areas of physics. Theorists working on improving calculations that describe these systems are interested in comparing the outcome with experimental results. In the same way, many theoretical results have spurred the experimental work to verify or disprove the predictions. One such example is the measurement of the electron affinity of calcium by D. J. Pegg *et al.* [20]. Prior to that measurement it had been generally believed that all negative ions of the alkali earth group elements were unstable, as this was known to be the case for both Be and Mg. Using electron spectrometry Pegg *et al.* measured an electron affinity of 0.043(7) eV. The measured affinity was supported by a multiconfiguration Hartree-Fock calculation by Charlotte Froese Fischer and co-workers, who confirmed the stability of the Ca^- ion and calculated that the $4s^24p$

^{2}P state in the calcium negative ion is bound by 0.045 eV with respect to the ground state of the Ca atom. This was in excellent agreement with the experimental value of Pegg *et al.* and the experiment was published back to back with the calculation in Physical Review Letters in 1987 [20, 21]. Many calculations followed these publications, most of which calculated electron affinities for Ca^- between 0.045 and 0.82 eV. Later, when the affinity was remeasured by Walter and Peterson in 1992 [22], making use of the more sophisticated technique of threshold spectroscopy with collinear beams, it was found that the value measured in 1987 was wrong. They reported an electron affinity of 0.0184(25) eV which soon was supported by two independent experiments - the first one being a dissociation experiment performed with a tandem accelerator and yielding an electron affinity of 0.0175(40) eV [23], the other being a lifetime measurement in a storage ring which did not agree with an electron affinity of 0.045 eV but was consistent with the lower affinity [24]. This subsequently triggered a new wave of calculations, refining the incorporation of the electron correlation and yielding lower electron affinities. The electron affinity was finally settled as 0.02455(10) eV by Petrunin *et al.* [25].

In atmospheric sciences, negative ions are known to balance the positive ion charge in the D-layer of the lower ionosphere at least to the same extent as the free electron [26]. Astronomers have found negative ions in stellar atmospheres and comet tails. Positive ions have been observed in interstellar clouds by radio astronomers for a long time [27] but the observations of the predicted negative ions have not been made until just recently. One reason for this is that high-resolution data of the rotational spectra for the more abundant anions have not been available earlier. Hence there has not been any possibility to correctly identify the more abundant species and the search has concentrated on well-characterized molecular anions with a very low rate coefficient for electron attachment [28]. In 2006 the carbon chain anion C_6H^- was identified in the laboratory as well as in the dense molecular cloud TMC-1 [28]. This observation was followed in 2007 by the identification and detection of the C_8H^- ion in the same interstellar cloud [29] and in 2008 by the detection of C_5N in the envelope of the carbon star IRC +10216 [30].

1.3 Applications of Negative Ions

In plasma etching the use of ion-ion plasmas, where the charge balance is kept by positive and negative ions, as opposed to positive ions and free electrons, is superior to the latter in etching quality [31]. At the same time there is a search for new, more efficient and in particular more environmentally friendly etching gases to use in these plasmas. The properties of the negative ions involved are important factors to consider in the modeling preceding any large-scale industrial investment [32]. Another field with interest in negative ions is Accelerator Mass Spectrometry (AMS), in which traces of rare isotopes with abundances down to 10^{-14} are detected. Negative ions can also be used as

the primary ion beam in Secondary Ion Mass Spectrometry (SIMS), a technique used in materials science and surface science to analyze the composition of solid surfaces and thin films. By sputtering the surface of the specimen with a focused primary ion beam and collecting and analyzing ejected secondary ions, a mapping of the surface composition can be carried out. The most commonly used negative primary ion beam is O^- [33]. In the attempt to make fusion a stable future energy source, the H^-/D^- ion has an important role. The fusion will take place in a plasma which is confined in a toroidal magnetic field, a so-called tokamak. The international experimental fusion reactor ITER is planned to be built in ten years' time and the main facility will be a large tokamak. In order to reach the temperatures where fusion will take place, heating of the plasma is provided by neutrals accelerated to high energy as ions. Therefore, large quantities of H^-/D^- that are accelerated, and then neutralized by collision or photodetachment, will be needed. The negative ion sources for ITER will have to deliver 40 A of negative ion current [34]. The development of such large-area, high-current sources is one of the keystones in the ITER project.

1.4 The Aim of the Thesis

This thesis is based on ten different scientific papers. They can be grouped into three different categories. The first four will deal with the structure of atomic negative ions. They will refine electron affinity values or reveal new structures of the elements under study. The second group is represented by two papers, presenting three studies of negative ion dynamics. Here the lifetime of metastable excited states in three different elements is measured. The last group consists of four papers dealing with ways of utilizing laser photodetachment to eliminate interfering isobars or isotopes in mass-selected ion beams. The first two categories provide valuable information that will help to deepen the knowledge of atomic negative ions in general. The last group of papers provide an aid in the development of smaller or more sensitive mass spectrometers.

2

Fundamental Properties of Negative Ions

2.1 Atomic Negative Ions

A charged particle, such as the electron, does not feel any long range attracting Coulomb force from a neutral atom. If one only considers the first principles of electrostatics one might even wonder how the negative ion can exist at all. There is, however, a simple semiclassical model where the force that binds the negatively charged electron to the neutral atom can be easily understood. Although it is true that the electron is not attracted by a neutral particle, the electron will polarize the atom when it is brought near to the electron cloud surrounding the atom and this will induce an electric dipole moment. This induced electric dipole moment can in turn attract the electron, which then becomes trapped in an induced electric dipole potential. The energy the atom gains in this process is the binding energy of the negative ion or equivalently, the electron affinity (EA) of the neutral atom. The electron affinity is defined as the difference in the total energy (E_{tot}) between the ground state of the neutral atom A and the ground state of the corresponding negative ion A^-.

$$\mathrm{EA}(A) = E_{tot}(A) - E_{tot}(A^-). \tag{2.1}$$

The ground states are defined as the lowest hyperfine structure levels of A and A^-, respectively. Equation 2.1 implies that a positive electron affinity means a stable negative ion.

Since there is no Coulomb potential that binds the extra electron, the electron has to stay close to the atom to remain bound. Thus, the negative ion becomes a much more fragile system than most positive ions and neutral atoms. The induced dipole potential that is responsible for the binding energy of a negative ion is proportional to r^{-4} while the coulomb potential that binds the electrons in the neutral atom is proportional to r^{-1}, where r is the distance from the center of the nucleus. This dissimilarity in binding potential behaviour gives rise to a number of differences between negative ions and atoms or positive ions. The electron affinity is about one order of magnitude lower than the

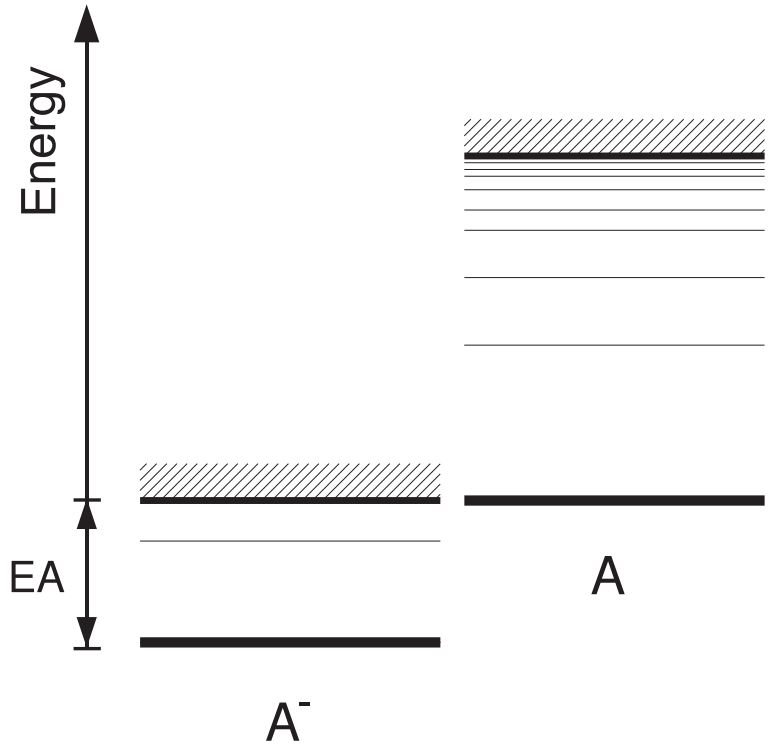

Figure 2.1: A schematic drawing of the energy levels in the hypothetical negative ion A^- and its corresponding atom A

ionization energy for the atom. For example, the EA of H is only 0.75 eV while its ionization potential is 13.6 eV. This short-range potential can only support a finite number of states (if any). In most cases only the fine-structure components of one term or sometimes two or three term splitting components of the ground state configuration are bound. In contrast, the Coulomb potential supports an infinite number of bound states, converging into a Rydberg series at the ionization threshold.

Early calculations of negative ion binding energies were often made by extrapolating known ionization potentials of neutral atoms and positive ions isoelectronic with the negative ions. These correctly showed that no stable negative ions could be expected to exist for elements like He, N, Ne, Mg, or Ar, but they generally underestimated the binding energies of the stable negative ions. These extrapolations therefore predicted that several negative ions that today are known to be stable, should be unbound. Quantum mechanical calculations within the independent particle model also fail to predict correct results even for the simplest negative ion H^-. The part of the binding energy that stems from the correlated motions of the electrons is much higher, and consequently more important, in the negative ion than in the atoms and positive ions, where

the Coulomb attraction is by far the dominating force. It is thus necessary to include the electron correlations in the calculation to be able to predict the correct electron affinity. Today, calculations are more trustworthy and an illuminating example is Charlotte Froese-Fischer's calculations of the metastable excited state lifetimes described in paper **V**. Other calculations associated with this work are the calculations on the structure of the cerium negative ion carried out by Beck an O'Malley [35] and the calculations of the detachment energy for HfF_5^- and WF_5^- reported by Hongshan Chen [36].

Although theoretical models have greatly improved over the years, the most accurate values of electron affinities are still those which are experimentally obtained. The one exception from this is the hydrogen ion as this three body system can be very accurately calculated [37]. For a long time the negative hydrogen ion was also considered the prime candidate for an atomic doubly charged negative ion. Its observation was even reported in a paper by Peart *et al.* [38] but subsequent experiments have failed to repeat this observation and atomic dianions are today not considered to be existing [39].

Even if detailed calculations are complicated, some crude but qualified guesses can be made of an element's electron affinity even without advanced calculations by looking at the periodic table and the filling of electronic shells in the elements. The halogens will, by acquiring an extra electron, gain a complete shell and these elements are consequently those with the highest electron affinities, while the alkaline earth metals have very low, and in some cases negative, electron affinities because the extra electron has to occupy a new sub-shell. This gives at least an idea of what to expect but it does not intuitively explain why, for example, nitrogen does not form a stable negative ion.

2.2 Molecular Negative Ions

The progression from atoms to molecules complicates matters. The situation is depicted in Fig. 2.2. The electron affinity of a molecule is defined, in the same way as for atoms, as the difference in the total energy between the neutral and the negative ion's ground states. This transition is often referred to as the "Adiabatic EA". In many cases, however, this transition is not the most likely to occur. If the lowest energy state of the neutral involves a rearrangement of the molecular structure, an instantaneous transition between the ion's ground state and some ro-vibrational state in the neutral could be the most probable transition. This is then referred to as the "Vertical Detachment Energy" (VDE). The corresponding transition from the neutral into the negative ion without rearranging the spatial structure of the molecule is called the "Vertical Attachment Energy" (VAE). These transitions are shown explicitly in Fig. 2.2. If the neutral molecule, as in the case of HfF_5, is unstable and quickly dissociates when the negative ion is neutralized, the adiabatic EA and VAE may not even be measurable quantities. Molecular

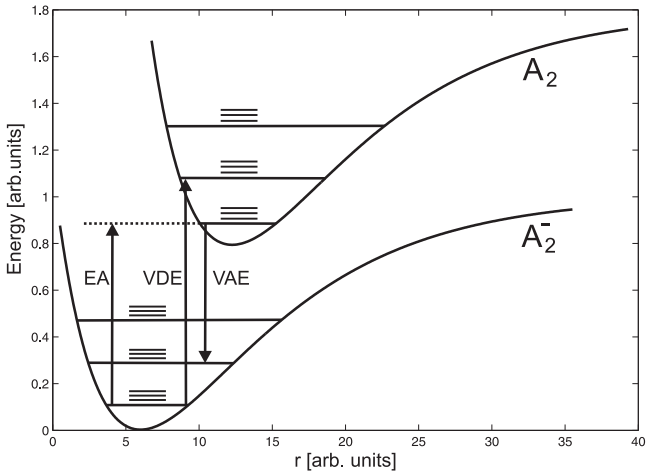

Figure 2.2: A schematic representation of the diatomic molecular potentials for the hypothetical molecule A_2. The transitions shown are the Adiabatic Electron Affinity or simply EA, the Vertical Detachment Energy (VDE) and the Vertical Attachment Energy (VAE), respectively. The vibrational and rotational excited levels are shown as horizontal lines in the potentials.

negative ions offer more possibilities for the electrons to relocate and share the extra charge. It is therefore possible to create stable dianions for molecules of large sizes and even trianions for large metal clusters. (Se ref. [40] and references herein.) Small dianions such as HPO_4^{2-} and SO_4^{2-} are common in solutions, such as body fluids, where they are stabilized by the environment. In the gas phase these ions auto-detach very fast but can be detected as resonance structures in the reaction cross sections for electron collisions. Metastable molecular dianions as small as B_2^{2-} and C_2^{2-} have been observed in this way [41].

3

Interaction Between Negative Ions and Photons

A photon that is absorbed by a negative ion can, if the photon energy is high enough, lead to the photodetachment process

$$A^- + \gamma \rightarrow A + e^-. \tag{3.1}$$

This process can be detected, sometimes by the absorption of photons, as is the case in the solar atmosphere, or by the detection of either the detached electron or the neutral atom. The relationship between the detected signal and to the photon energy will give information about the structure of the negative ion. There are a number of experimental methods to achieve this and they will be briefly outlined later in the text. The probability for photodetachment is measured as a cross section, and is a function of photon energy. The general behavior of the cross section is discussed next.

3.1 The Photodetachment cross section

The probability, P_d, for a transition from the initial state $|\psi_i\rangle$ to the final continuum state $\langle\psi_f|$, due to the interaction between an atom and a photon, is described by Fermi's golden rule:

$$P_d = \frac{2\pi}{\hbar}|\langle\psi_f|D|\psi_i\rangle|^2\rho_f, \tag{3.2}$$

where D is the electric dipole coupling operator, which corresponds to the photoabsorbing process, and ρ_f is the density of final states in the continuum. ρ_f is proportional to the energy of the ejected electron, ε, as

$$\rho_f \propto \sqrt{\varepsilon}. \tag{3.3}$$

After photodetachment it is possible reduce the problem to one dimension and describe the system containing the free electron and the residual atom after photodetachment by an effective potential, V_{eff}, expressed as [42]

$$V_{eff}(r) = V(r) + \frac{\hbar^2}{2\mu r^2} l(l+1). \tag{3.4}$$

Here $V(r)$ is the potential due to the atomic core and the second term is the centrifugal part of the potential where *l* is the angular momentum of the outgoing electron, μ is the reduced mass, and *r* is the distance between the electron and the core of the residual atom. The threshold behavior is determined by the long range behavior of the potential, which is justified by the low velocity of an electron detached by photon energies in the threshold region. The low velocity then consequently means that the electron spends a long time in the region of large *r*. The interaction between the departing electron and the neutral, $V(r)$ in Eq. 3.4, in a negative ion is the induced dipole potential, which falls off as r^{-4}. At large *r*, it is then the centrifugal barrier term that will be the dominating term in Eq. 3.4. Therefore, the Eqns. 3.2 and 3.3 will eventually lead to a cross section behavior described by

$$\sigma \propto k^{2l+1}, \tag{3.5}$$

with k being the linear momentum and l the angular momentum of the outgoing electron, respectively. This is referred to as the Wigner threshold law and was given a much more rigorous treatment in Eugene Wigners article in 1948 [43]. Equation 3.5 can be expressed more conveniently as a function of photon energy. If an electron is photodetached by a photon with an energy $E = \hbar\omega$ from a system with a photodetachment threshold energy E_{th} its kinetic energy will be $E_k = E - E_{th}$. The cross section dependence (3.5) will then take the form

$$\begin{cases} \sigma(E) \propto (E - E_{th})^{l+\frac{1}{2}} & \text{when} \quad E > E_{th} \\ \sigma(E) = 0 & \text{when} \quad E < E_{th} \end{cases} \tag{3.6}$$

The Wigner law in this form is of crucial importance to Laser Photodetachment Threshold Spectroscopy (LPTS), as will be discussed in the next section. From Eq. 3.6 it can be seen that when the angular momentum of the ejected electron is zero the cross section will have an inverse square root behavior at the threshold as indicated by the dashed line in Fig. 3.1. This behavior is generally called an s-wave. Since the photon has an angular momentum, l, of 1, the quantum mechanical selection rule

$$\Delta l = \pm 1. \tag{3.7}$$

state that the total angular momentum of the system after photodetachment must change by the same amount. If the photodetachment does not involve any excitation of the neutral or inner shell detachment this extra quantum of angular momentum is carried away by the detached electron. A detached electron which in the negative ion occupied an s-state, where $l = 0$, will leave the ion with an angular momentum, $l = 1$. The solid

line in Fig. 3.1 represents this so-called p-wave. For an electron that had higher l in the negative ion, $\Delta l = -1$ will dominate near the threshold, as higher l contributions will be suppressed by the centrifugal barrier.

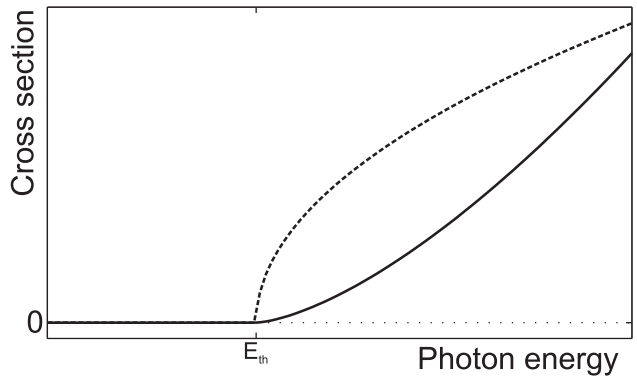

Figure 3.1: The photodetachment cross section shape close to the threshold for an s- and a p-wave, represented by the dashed and the solid lines, respectively

The Wigner law is only valid within the threshold region for photodetachment. There is little theoretical guidance of the actual length of validity and the law is often said to hold if the deviation between the law and reality is "less than some arbitrary fraction" [42]. The Wigner law can be seen as the first term in the expansion of an (unknown) exact solution expressed in increasing powers of k. The first term in this expression is referred to as the Wigner term and the second as the leading correction. At higher energies, the leading correction in the expansion becomes important and Eq. 3.5 is no longer valid. The form of the leading correction has been calculated by several different approaches. In the derivation of the Wigner law any potential falling off faster than r^{-2} was neglected whereas O'Malley included a correction term corresponding to the induced dipole potential [44]. Farley has used a semi empirical analytical calculation to derive a correction which is identical to O'Malleys in the limit of small polarization [42]. Both these approaches give better descriptions of the cross section dependence when the photodetachment process has progressed beyond the threshold region.

With the exception of the threshold region there is no analytical expression that can be used to describe the variation of the photodetachment cross section as a function of photon energy. The general shape over a wide range of photon energies is shown in Fig. 3.2. Starting at zero at the threshold, the photodetachment cross section rises with increasing photon energy as the density of states increases and as the electron is able to pass above the centrifugal barrier. At higher photon energies, the cross section drops off towards zero as the overlap integral of the initial wave function and the rapidly

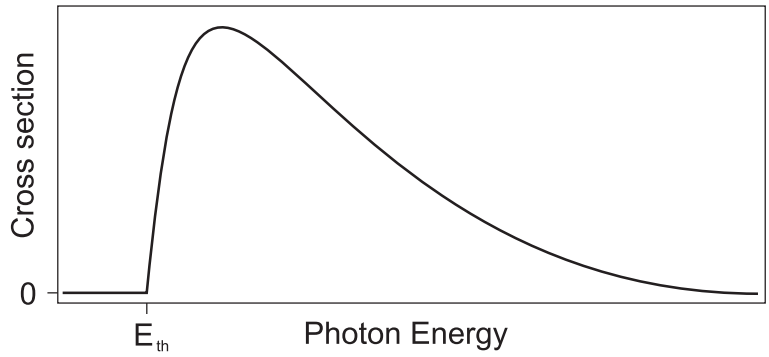

Figure 3.2: The general behavior for the photodetachment cross section over a wide range of photon energies.

oscillating wave function of the emitted electron tends to zero. Obviously, the cross section should reach a maximum value somewhere in between these two extremes. A compilation of negative ions where the photodetachment has been investigated over a large energy range reveals that the peak occurs at an excess energy that ranges from 2 to 5 times the energy of the threshold. It would, of course, be interesting to be able to estimate the photon energy at the peak of the cross section. To do so, we then assume that the outermost electron in a negative ion is bound in a square well potential which as a finite depth. The maximum overlap between the initial wavefunction and the wave of the outgoing electron will then occur when the deBroglie wavelength of the outgoing electron, λ_e^{db}, matches the size of the negative ion. In the situation when an electron lying in an s-orbital in the negative ion is emitted, the phase of the initial wavefunction will be the same over the whole negative ion. Using this argument, the largest overlap will then occur when $2\langle r\rangle = \frac{\lambda_e^{db}}{2}$, i.e. when $\langle r\rangle = \frac{\lambda_e^{db}}{4}$. In the case of a negative ion with a p-wave valence electron the situation is different since this is an odd wavefunction. The maximum overlap occurs here when $\langle r\rangle = \frac{\lambda_e^{db}}{2}$. In other words, at the peak of the cross section the relation

$$\lambda_e^{db} = \xi\langle r\rangle \tag{3.8}$$

should hold. Here ξ is 4 or 2 depending on whether the valence electron is an s- or p electron, as discussed above. To find the photon energy where the cross section peaks this relation is inserted in the expression relating the photon energy to the deBroglie wavelength for a photodetached electron:

$$E_{\sigma_{max}} = \left(\frac{h}{\xi\langle r\rangle}\right)^2 \cdot \frac{1}{2m_e}. \tag{3.9}$$

Here $E_{\sigma_{max}}$ is the photon energy at the peak of the cross section, h is Planck's constant, m_e the electron mass, and $\langle r\rangle$ is the radius of the negative ion. In expressions 3.8 and 3.9

it is assumed that the full energy of the photon is converted in to energy of the electron. This is justified since we are interested in the deBroglie wavelength of the outgoing electron in the region where it overlaps with the initial wavefunction. As the electron reaches large distances, it will loose energy and consequently the deBroglie wavelength will increase. Using expression 3.8, we can calculate the size of the negative ion from known photodetachment crossection values and plot the result together with the radius of the ions from direct experimental data. This is shown in Fig. 3.3.

First we observe that this very simple model is able to predict the size of the atom directly from the energy at which the photodetachment cross section has its peak. It should be noted that the values presented are the size of the negative ion on an absolute scale, and no fitting parameters have been used. Second, we find that the model is able to very accurately predict the increase of the size of the ions as we descent within one group in the periodic table. At this stage, we have data for $\langle r \rangle$ and photodetachment cross sections for alkali and halogen negative ions [45–50]. It is likely that the model works particularly well here since negative ions in both groups have closed shell structure. It would, of course, be interesting to extend the model to investigate the full periodic table.

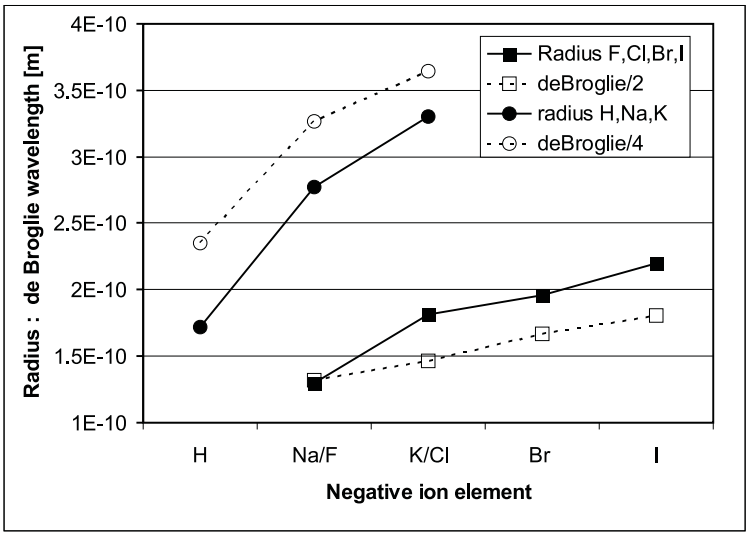

Figure 3.3: The radius of $\langle r \rangle$ of negative ions. Filled points represent direct experimental determinations, and open points represent estimations using 3.8

3.2 Selection Rules

The absorption of a photon by an atomic system is only possible if certain quantum-mechanical conditions are fulfilled. These conditions are the same quantum-mechanical selection rules as those for excitation or ionization of neutral atoms. The photon carries an angular momentum of 1 and thus has parity π = -1, according to $\pi = (-1)^{\sum l}$, here $\sum l$ is the sum of the angular momentum for all electron in open shells. Thus an electric dipole transition will only connect states with opposite parity. Other selection rules to take into consideration are:

$$\Delta J = 0, \pm 1; 0 \leftrightarrow 0 \text{ forbidden}, \tag{3.10}$$

$$\Delta M_j = 0, \pm 1, \tag{3.11}$$

$$\Delta L = 0, \pm 1; 0 \leftrightarrow 0 \text{ forbidden}, \tag{3.12}$$

$$\Delta S = 0. \tag{3.13}$$

Equations 3.12 and 3.13 are only strictly valid in the case of pure LS-coupling. One should keep in mind that these selection rules refer to the initial state of the negative ion, not including the photon, while the final state consists of the total final system, including both the neutral atom and the free electron. The atom-plus-free-electron system will have more possibilities to fulfill the selection rules than in a bound-bound transition. The parity condition just mentioned and the fact that the excited states in negative ions are of the same parity as the ground state makes ordinary spectroscopy impossible for negative ions. Ordinary spectroscopy here means the detection of the photons emitted as excited systems relax, the method which has been used to collect most of our information on the structure of atoms and positive ions.

3.3 Resonance Structures

Resonance structure in the photodetachment spectra generally arises from photoexcitation of unbound excited states in the negative ion. These unbound states lie embedded in the continuum above the detachment level and will autodetach rapidly upon excitation. The resonances are traditionally classified as being either Feshbach or shape resonances [19]. Feshbach resonances correspond to states that lie energetically below the parent state in the neutral atom and have therefore usually a longer autodetachment lifetime (and a smaller width) than the shape resonances, which are associated with states that lie above the parent state. There is also a small possibility to photo excite from a low-lying bound state to a high-lying bound state in the negative ion via higher order processes. Such a state can not autodetach since it lies energetically below the atomic ground state. It can, however, subsequently absorb an additional photon and photodetach. The result

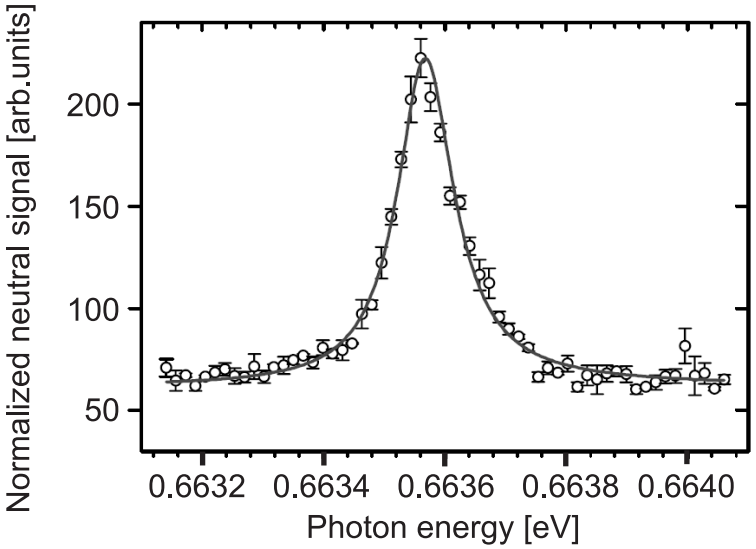

Figure 3.4: A resonance structure found in Ce^-. This resonance is positioned above the ground state detachment threshold situated at 0.65 eV [**III**].

is a resonance peak in the background below the photodetachment threshold. Bound-bound transitions have been studied using multiphoton techniques or M1 transitions for negative ions of several elements [17, 51, 52]. Only in the Osmium negative ion has a resonance that demonstrates the existence of a bound state of opposite parity [53] been observed. Paper III represents a second case where a state of opposite parity is most likely to be present. Figure 3.4 is an example of resonant structure found close to the ground state threshold in Ce^-.

4

Photodetachment: Experimental Methods

Negative ions have been studied by different photodetachment techniques since the mid 1950's. The first observation of the photodetachment of negative ions in a laboratory was recorded by L. M. Branscomb and W. L. Fite in 1953 [6]. The first detailed study of a *photodetachment cross section* was reported by Branscomb *et al.* in 1955, using a tungsten lamp and a beam of negative hydrogen atoms [7]. The same technique was also used by the same authors to attain the first *photodetachment threshold measurement* on O^- [54]. The broad spectral features of the tungsten lamp had to be narrowed using a series of sharp cut off filters. Photodetachment experiments have gained enormously from the invention of the laser which provides monochromatic light of known wavelengths and the development of tunable lasers have pushed the field even further. The laser made the photodetachment technique the most exact way of measuring electron affinities. The three main techniques are, Laser Photodetachment Electron Spectroscopy (LPES), Laser Photodetachment Threshold Spectroscopy (LPTS), and Laser Photodetachment Microscopy (LPM). In LPES and LPTS, pulsed lasers are used in order to increase the photon fluence during the illumination and consequently increase signal yields. This also facilitates a time-gated detection scheme which discriminates against a continuous background collision-signal and improves the signal to noise ratio. The LPM measurements are performed with a Continuous Wave (CW) laser. The trade off for the pulsed lasers lies in the bandwidth of the light. While CW lasers can easily have a spectral line width in the order of 10^{-5} cm^{-1} the typical pulsed lasers have bandwidths of the order of 10^{-1} cm^{-1}.

4.1 Laser Photodetachment Electron Spectroscopy

A typically LPES measurement setup is illustrated in Fig. 4.1. A laser with a photon energy higher than the electron affinity intersects an accelerated beam of negative ions at an angle of 90°. The energy distribution of the photodetached electrons is measured, either by time of flight [55] or by electrostatic deflection [56]. The energy of the electrons

will correspond to the difference in energy between the photon energy and the energy of the transition from the initial state of the electron to the final state of the residual atom:

$$E_e = E_\gamma - (E_{final} - E_{initial}) \tag{4.1}$$

By comparing the energy of the detected electrons to the known energy levels of the element's neutral atom, the electron affinity and the energy of excited states can be extracted. The electron spectroscopy can reveal the whole structure of the negative ion, providing that all excited states are populated. More information about the structure of

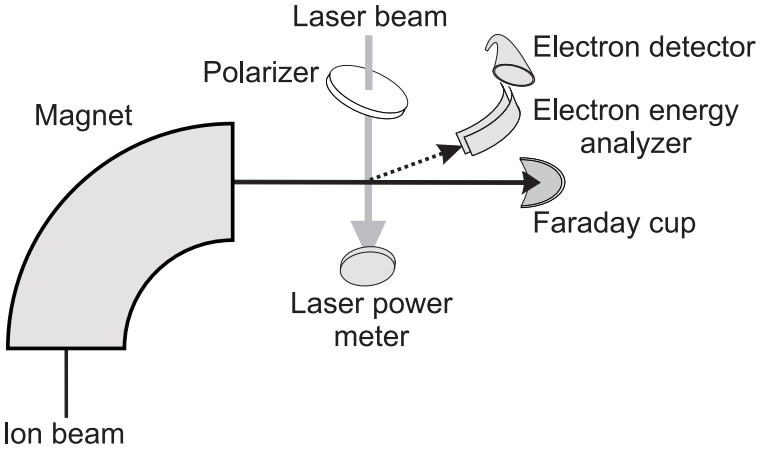

Figure 4.1: A typical laser photodetachment electron spectroscopy setup. Electrons are energy analyzed and guided into a detector. The laser beam can be polarized to examine the angular distribution

the negative ion can be extracted if the laser light is linearly polarized. The angular distribution of the electrons can be measured and the ejected electron's angular momentum can then be determined. From the relationship between the signal at a specific angle and the linear polarization angle the so-called asymmetry parameter can be found. The value of this parameter depends on the relative amplitudes between the s and the d -wave in the case of a detached p electron [56, 57]. In the case of a detached s electron there is a pure p-wave detachment and the β parameter becomes a constant. The behavior of the asymmetry parameter in comparison with theoretical models can give valuable information about the electronic structure of heavy atomic negative ions. The angular distribution can also be used as a means to direct the released electrons towards the detector, such that a higher yield of signal can be achieved [58]. The energy resolution for any kind of electron spectrometer is several orders of magnitude lower than for threshold spectroscopy using tuneable lasers. This puts a limit to the level of accuracy that can be achieved for the measured energies.

4.2 Laser Photodetachment Threshold Spectroscopy

In LPTS the photon energy is varied over the threshold region for photodetachment. The yield of photodetachment signal as a function of photon energy is recorded and the data obtained is used to fit the Wigner law (Eq. 3.6). From the parameters of this fit both the angular momentum of the outgoing electron and the photodetachment threshold value can be extracted. The detected signal is either photodetached electrons or the residual neutral, where the latter tends to be the more common choice. LPTS experiments can be done in a cross-beam configuration, where the laser is applied at a 90° angle to the accelerated ion beam. Under the condition that the angle between the two beams is exactly 90°, this will give a Doppler free photodetachment threshold. The Doppler shift of the light, ω, is proportional to the velocity of the ions, ν, and the cosine of the interception angle, θ, between the laser beam and the fast moving ion beam according to the relativistic Doppler formula:

$$\omega' = \omega \frac{1 - \frac{\nu}{c_0} cos\theta}{\sqrt{1 - \nu^2/c_0^2}}. \tag{4.2}$$

The cosine dependence means that the result is very sensitive to even small deviations from 90°. A crossed beam measurement is limited in resolution by the Doppler shift induced by the divergence in both the laser and ion beams. This causes Doppler broadening to be of the order of 10^{-1} cm^{-1} for a beam originating from a cesium sputter source. Doppler broadening is reduced by more than a factor of 100 if a collinear geometry such as illustrated in Fig. 4.2 is used [59]. The ions to leave the sputter source with a substantial longitudinal energy spread. This spread is significantly reduced due to kinetic compression of the fast accelerated beam [60], so that its contribution to the Doppler broadening becomes negligible. In order to eliminate the induced Doppler *shift*, a correction must be made for the measured threshold. For low resolution experiments it is sufficient to calculate this using the non relativistic Doppler formula with $\theta = 0$,

$$E_{p,a} = E_0 \left(1 \pm \frac{v}{c}\right), \tag{4.3}$$

where $E_{p,a}$ is the Doppler shifted energy where the subscript stands for parallel or anti-parallel, E_0 is the Doppler free energy, v is the ion beam velocity and c is the velocity of light. To correct for the shift in a high-resolution experiment, threshold measurements for both parallel and anti-parallel ion and laser beams must be performed. After the threshold values have been extracted from the respective fit of the Wigner law, the Doppler free threshold can be obtained by taking the geometric mean of the two values [61]:

$$E_0 = \sqrt{E_p E_a}. \tag{4.4}$$

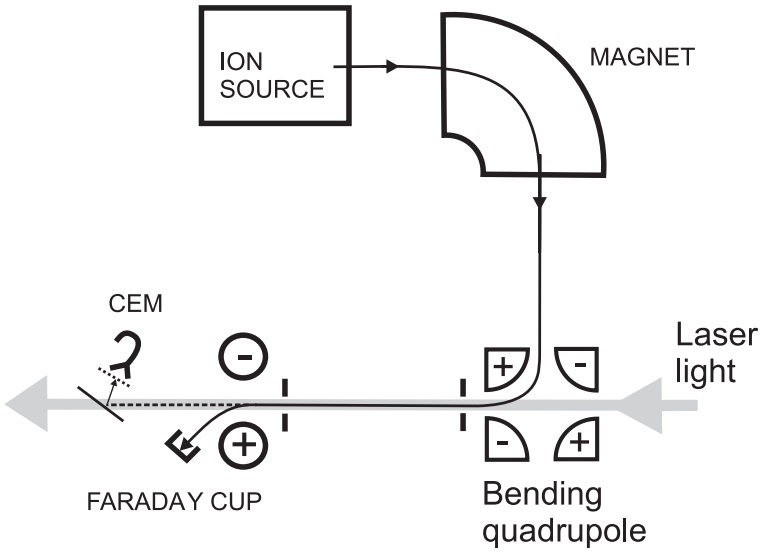

Figure 4.2: A collinear setup used for laser photodetachment thresholds spectroscopy studies.

4.3 Laser Photodetachment Microscopy

In LPM the spatial distribution of the electrons photodetached in the presence of an uniform electric field is imaged directly. A typical setup is illustrated in Fig. 4.3. Provided the electric field is small compared to the electric field of the atom, the electron is emitted from the ion in the form of a spherical wave of energy E_k. The electric field makes this wave fold back in the direction of the field and interfere with itself. This interference produces a ring pattern when the electrons are detected perpendicular to the field. The number of rings or the accumulated phase (Φ) is a function of the electrons initial kinetic energy (E_k):

$$\Delta\Phi = \frac{4\sqrt{2}}{3}\frac{\sqrt{m}}{\hbar q F}E_k^{3/2}, \tag{4.5}$$

where q is the elementary charge, m the electron mass, and F the applied electric field [62]. The electric field and the photon energy are well known so the kinetic energy of the electrons can be found by fitting Eq. 4.5 to the experimental data. Since

$$E_k = \hbar\omega - E_{th}, \tag{4.6}$$

the electron affinity of the neutral species can be easily extracted. It is important to note that the photon energy has to be known precisely and since this technique demands a cross-beam geometry, any ambiguity in the 90° angle must be treated. This problem has been solved by the group at Laboratoire Aime-Cotton [62] by deliberately overlapping

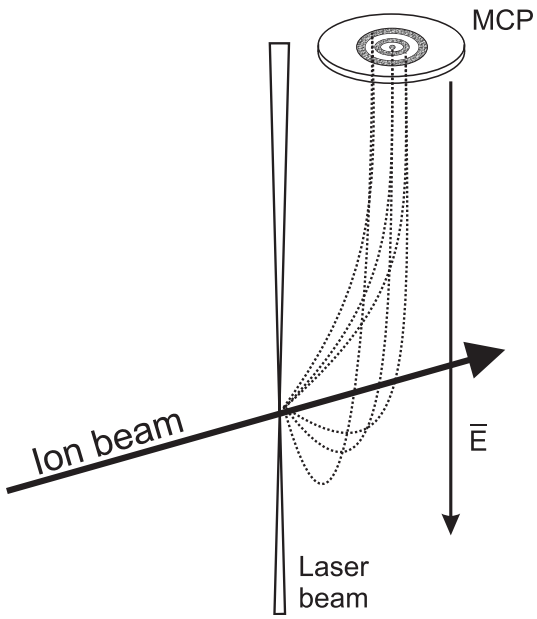

Figure 4.3: The principle for the laser photodetachment microscope.

the beams at an angle different from 90° and then retro-reflect the light so that two separate sets of interference patterns can be detected. Measuring the distance between these patterns, D, and knowing the distance to the retro-reflecting focusing mirror, f (practically the mirror focal length if the intercepting angle is close to 90°), it is possible to calculate and extract the Doppler free electron affinity from the triangular geometry of the setup from the expression:

$$E_{th} = \gamma \left(1 + \beta \frac{D}{2f}\right) h\nu - \frac{E_{k_i} + E_{k_r}}{2}. \tag{4.7}$$

The accuracy of the electron affinities measured with the LPM method has reached values of 0.0016 - 0.0024 cm^{-1} [17].

The drawback of the photodetachment microscope is that the method will only work provided that the kinetic energy (E_k) is low enough, i.e., in the 0.01 - 0.4 meV region [62]. This limits the technique to those ions that have a relative high yield of photodetachment signal even close to the threshold, in other words, the s-wave detaching ions.

5
Mass Spectrometry

When J. J Thomson discovered the possibility to separate anode rays into different elements by means of their different mass to charge ratio, he founded the field of mass spectrometry. In 1898, W. Wien had already used a strong magnetic field and deflected the rays that could be seen streaming out through the holes of a pierced cathode in a vacuum tube, the anode rays or, for Wien, *die kanalstrahlen*. He could only conclude that they were positively charged but his work was the starting point for Thomson who realized that these rays were formed by many different particles and hence looked for a way to separate them. He found that he could detect the particles by letting them strike a photographic plate which was placed at a right angle to their path. Prior to the photographic plate, he sent the beam through a magnetic and an electric field which then separated the beam into a multitude of fan shaped beams, each one representing a specific mass to charge ratio. The fan like spread of the beam arises from the velocity distribution of the particles which with a given value of e/m will strike the photographic plate in a specific parabola. Knowing the e/m of one of these parabolas one could calculate the e/m of all the others. This was the first mass spectrometer and it had an advantage over the usual spectrum analysis in that it would immediately give the mass to charge ratio of a detected particle. In was this way Thomson could see that also some of the particles produced when passing through the cathode had a negative charge.

Today the art of mass spectrometry has been refined to become an incredibly sensitive tool. Maybe the best known example is the detection of ^{14}C used in the dating of organic materials. In addition to the two stable isotopes; ^{12}C and ^{13}C, carbon also has several radioactive isotopes, all very short lived (from 14 ms for ^{20}C to 20.5 minutes for ^{11}C) except ^{14}C. This radio-isotope has a half life of 5730$\pm$40 years and decays by emitting a β-particle, producing ^{14}N. It is continuously produced in the upper ionosphere by cosmic radiation such that the amount of ^{14}C in the air we breath is about 10^{-12} to that of ^{12}C. Due to the respiratory process, the carbon content of all living organisms is constantly renewed. Therefore, as long as an organism is alive its ^{14}C content is equal to that of the surrounding respiratory media. When the organism dies its carbon content is no longer renewed and the amount of ^{14}C starts to decrease due to the decay of the

radio-isotope.

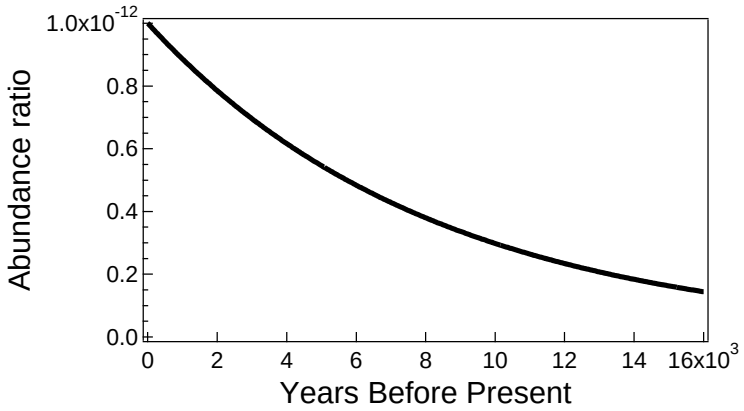

Figure 5.1: The decay curve of ^{14}C

The first person to suggest that the ratio of ^{14}C to ^{12}C could be used as a chronographic marker was Willard F Libby who demonstrated the presence of ^{14}C in living matter in 1947 [63]. Libby and his group continued to developed their technique during the 1950's and he was awarded the Nobel Prize in chemistry in 1960 for his work [64]. By measuring the ratio of $^{14}C/^{12}C$ in any historical artifact that contains some organic material, its age could be determined (Fig. 5.1). In Libby's days, the only way of measuring the ^{14}C content was to do a radiological measurement, i.e. measuring the activity of the sample with a Geiger counter. In order to get a useable signal the sample had to be large and the measurment time was very long. Acquisition times in the order of days was not uncommon as one gram of contemporary carbon will give about 10 counts per minute. When the technique was refined and became a reliable standard the awareness grew that the natural abundance of ^{14}C was after all not constant. Control measurements from dendrochronology[1] showed a discrepancy from the absolute decay curve of modern day carbon and revealed the need of a calibration curve. The amount of carbon in the atmosphere undergoes small but significant fluctuations due to changes in the intensity of the Earth's magnetic field and modulations of the cosmic-ray flux by solar activity. In addition, testing of nuclear weapons in the 1960's caused a spike in the ^{14}C production. To deal with all these variations a calibration curve using alternative dating methods such as dendrochronology and ice cores, was established. The second revolution in ^{14}C measurements science was the discovery of a means to count the number of ^{14}C *atoms* as opposed to the number of ^{14}C *decays*.

[1]The method of scientific dating based on the analysis of tree-ring growth patterns.

5.1 Accelerator Mass Spectrometry

The sensitivity increase gained by counting the ^{14}C atoms instead of their decay is roughly 10^4. This implies that dating of modern carbon can be done with submilligram samples. In addition to the severe difficulties of obtaining the sensitivity needed for detecting an ultra-rare isotope such as ^{14}C, conventional mass spectrometers lack the selectivity to discriminate against the extremely close isobar ^{14}N ($\Delta_{m/m} = 1.2 \times 10^{-}5$). The problem was solved in 1977 by two independent groups who both realized that in Accelerator Mass Spectrometry (AMS), where the injected particle is a negative ion, there would be a natural discrimination against any nitrogen contamination due to its inability to form a stable negative ion [65, 66]. Both groups used Van der Graaf tandem accelerators for their measurement, where the ions after a low energy mass selection are injected into a megavolt accelerator tube. The ions are accelerated towards a stripper on a high potential and are there stripped to form highly charged positive ions. These ions are accelerated further towards detectors at ground potential. One of the groups, D. E. Nelson *et al.* proved without doubt that the particle counting technique was able to detect and measure the abundance of ^{14}C in modern carbon. The second paper, written by C. L. Bennet *et al.* showed that the technique had the power of dating very small samples of graphite as far back in time as 50 000 years before present. Tandem accelerators also have the advantage that any isobaric molecular ions are destroyed in the stripping process. With the development of analytical techniques performed by AMS, ^{14}C/^{12}C ratios of 10^{-15} can be detected. The size of the sample can be reduced by several orders of magnitude to less than 1 mg and still a sample of modern carbon will yield 10 000 counts in just a few minutes. AMS created a whole new research area in physics and cosmo- and geo-chemistry. It is now a possible to measure ultra trace, long-lived or stable isotopes such as ^{14}C used for biological dating [64],^{41}Ca and ^{59}Ni used for dating geophysical and extraterrestrial objects [67, 68], ^{36}Cl and ^{129}I, used for example to trace contamination from nuclear sites [69] and ^{26}Al used for biomedical tracing [70]. Many of these have such low activity that they would be virtually impossible to measure radiologically.

Today AMS is by far the most widely used tool in the search for ultra trace elements even though some competitive techniques have recently been developed, most successfully by the refinement of laser Resonance Ionization Mass Spectrometry (RIMS) [71]. The recent trend is towards smaller tandem machines which have a smaller investment cost and are easier to maintain [72, 73]. Several machines with terminal voltages ranging from 1 MV down to as low as 200 kV [74] have been built in recent years. The low terminal voltages only allow stripping of the negative ions into 1+ to 2+ charge states. For these low charge states the breakup of molecular isobars is not as effective and longer gas targets have to be used to ensure the effective suppression of molecules. Overall,

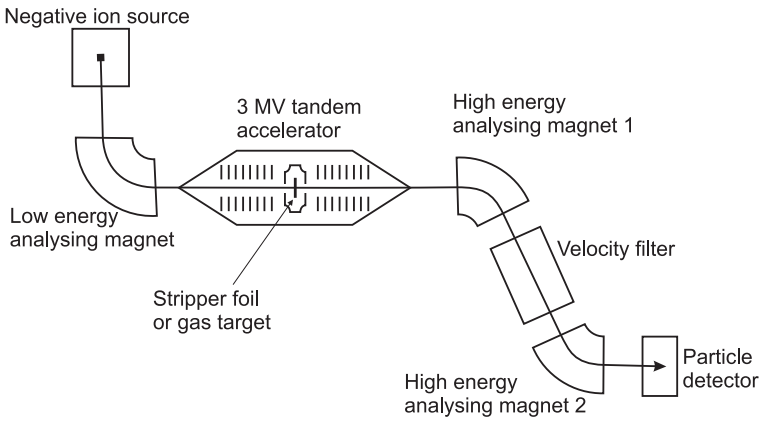

Figure 5.2: A typical AMS system

the problems due to interfering species in the beam grow as the terminal energies get smaller. Other means of suppression thus need to be investigated.

5.1.1 Laser Suppression of Beam Contaminants

The fragile nature of the negative ions that allows them to be neutralized by lasers could be used as one means of discrimination against contaminants in a mass-selected ion beam. This is especially interesting for AMS applications since negative ions are used in the injection stage. The requirement is that the contaminant must have a lower EA than the element of interest. This is fortunately the case for many interesting ultra-trace elements, shown by some examples listed in Table 5.1.

The first experiment to test this idea was performed by the group of Berkovits [75], who used the frequency doubled fundamental radiation from a pulsed Nd:YAG to demonstrate that it was possible to partially deplete a beam of S^- ions while leaving the Cl^- ions unaffected. In a subsequent measurement on Co^- the same group used the fundamental wavelength of a pulsed Nd:YAG laser to reach a degree of ion-beam depletion of just above 99 % [76]. In articles VII and VIII, included in this thesis, this concept has been extended to demonstrate how a laser of the right frequency can be used, when utilizing the induced Doppler shift of a fast moving ion beam, to selectively detect different isotopes of the same element. Although the depletion achieved by Berkovits *et al.* was as high as 99 %, their duty cycle was low due to the use of a pulsed laser. At the beam acceleration energy they used, 100 keV, the mass 59 u ions are traveling at a speed of about 570 000 m/s. Even with a 10 kHz laser, an interaction region of nearly 60 meters length would be required to apply light to all ions in the beam. This is both

Table 5.1: Some examples of ultra-trace elements of interest where laser light in principle could be used as a suppressor on the negative ion side of an AMS machine. Column 3 gives the difference in EA between the trace element (te) and the contaminants (c). ^{41}Ca is included as an example where the suppression would not work.

Trace element	Contaminant(s)	EA_{te} - EA_c [eV]	λ range [nm]
^{10}Be	^{10}B	0.011	4431.5 - 4275.5
^{14}C	^{13}CH, $^{12}CH_2$	0.024, 0.61	1000,5259 - 982.5
^{36}Cl	^{36}S	1.536	596 - 393
^{41}Ca	^{41}K	-0.476	N. A.
^{59}Ni	^{59}Co	0.633	1867 - 1072.5
^{92}Nb	^{92}Zr	0.467	2817 - 1442
^{137}Cs	^{137}Ba	0.321	8610 - 2632.5

hard to achieve and impractical and there are two more convenient methods available; either use a CW-laser or slow down the ions. The problem with CW lasers is that they do not provide sufficient photon flux to effectively deplete a beam of negative ions. The problem with a really slow beam of ions is that the beam would diverge too much after even a very short distance due to the emittance of the beam. An ensemble of ions traveling in a conservative field are subject to Liouville's theorem which states that the phase space volume of the ensemble is constant. The phase-space volume originating from the sputter source in practice makes a parallel beam impossible -a narrow beam will have a large angular spread while a parallel beam will be infinitely large.

Both these obstacles were solved by Y.Liu *et al.* who demonstrated the use of a gas-filled radio frequency quadrupole ion guide or "ion-cooler" on a beam of negative ions. This device is able to slow down and cool the ions[2] and can achieve a transit time of ms along the axis of the ion-cooler [77]. Since the decelerated ions travel in a narrowly confined beam along the quadrupole axis for such a long time, a very high fluence of photons is seen by each ion if a laser beam is applied through the quadrupole. A CW- or a high repetition pulsed-laser could now be used to clean the ion beam from contaminants with a 100 % duty cycle. When the remaining ions in the beam are accelerated again by a homogenous electric field the beam will be thermalized and the energy spread among the ions will be very low. The negative ion sputter sources notoriously produce a large high energy tail which limits the mass resolution of a mass separating magnet. The tests of the ion-cooler at Oak Ridge National Lab show that this tail is completely removed after passing through the cooler [78]. Paper X in this thesis, demonstrates that a very high degree of depletion is made possible even for a moderate power of the depleting laser. Both these abilities provided by the ion-cooler can be of great use in an ultra trace element detection scheme: The removal of the sputter source-induced high energy tail allows for a much better resolution between neighboring isotopes, and the high degree of removal of contaminating atomic and molecular isobars can now be realized for small, low voltage tandem accelerators.

5.2 The Search for ^{182}Hf

When a class O or B star has consumed most of its hydrogen it will enter the red giant phase. The remaining hydrogen shell expands and cools down while the core contracts and increases its temperature as carbon is formed from the fusion of helium atoms. As the core continues to increase in density and temperature, additional fusion processes are initiated and all elements up to iron are formed. When the core is essentially iron

[2]Liouville's theorem is not valid when dissipative effects, such as collisional cooling of beams, are present. Therefore it is possible to decrease the phase space volume of the ion ensemble and get a narrowly confined beam.

fusion stops, since energy is no longer gained by further fusion processes. Without the outward radiation pressure from the energy created in fusion, the star undergoes a sudden gravitational collapse. The core temperature rises to over 100 billion degrees as the iron core is compressed. Finally the repulsive forces between nuclei overcomes the gravitational forces and the core repulses outward in a shockwave. This great explosion can for a short moment be brighter than a whole galaxy and is known as a supernova explosion. All other elements heavier than iron are formed in this process and cast out through the universe together with the lighter elements. Some isotopes of heavy elements are only formed in supernovas and one of these is ^{182}Hf.

5.2.1 Supernova Tracing

When the remains of the exploding star are spread out some of them can be deposited onto planets. Among all of the elements within these remains, there will also be some ^{182}Hf. The number of a specific isotope (F_i) that would be deposited per unit area onto the Earth from a supernova shockwave passing our planet can be estimated by

$$F_i = \frac{M_{ej,i}}{4\pi A_i m_p D^2}, \tag{5.1}$$

Where $M_{ej,i}$ is the total ejected mass of isotope i from the supernova, A_i is the mass number of that isotope , m_p is the proton mass and D is the distance from earth to the event [79]. The half life of the ^{182}Hf isotope is 9 $\pm$ 2 million years so the the fluence must be corrected for decay to obtain present day numbers. The supernova-produced material deposited into the Earth's oceans will sink to the bottom and sediment in the deep sea crust. The sedimentation rate is known, so that a certain depth corresponds to a certain number of years. Thus, examination of this layers at different depths into the crust will tell how far back in time the material was deposited. There are some indications that our solar system resides in the interior of a supernova remnant [79] and ^{60}Fe, another isotope unique for supernovas, have been found at a crust depth corresponding to a supernova shock wave passing through the Earth 2.8$\pm$ 0.4 million years ago [80]. Although recent measurements show results inconsistent with the time span expected for the deposition from a shockwave of a nearby supernova [81], this nevertheless spurred the search for ^{182}Hf traces, to either verify or contradict the ^{60}Fe results.

Using theoretical estimates of the production rate and the known half-lifes of ^{60}Fe and ^{182}Hf, Eq.5.1 can be used, to first calculate the distance to the supernova and then to estimate the expected ^{182}Hf abundance in the given sediment layer. The predicted abundance of ^{182}Hf compared to ^{180}Hf for this specific supernova has been calculated to 10^{-13} [82]. For such small abundances the only possible tool for detection is an AMS machine. There is however an additional complication in the fact that the final decay product of the radioactive ^{182}Hf is the stable tungsten isotope ^{182}W.

5.2.2 Isobaric Suppression

As the signal from any two particles of the same mass and charge in a mass spectrometer will be indistinguishable[3] there is a need to suppress the tungsten isobar. The first step to reduce the ^{182}W is to perform a chemical separation of the sample. Hafnium and tungsten show different chemical properties and allow for effective chemical separation. The second step is to use a molecule that has a high production rate in the negative ion source in the hafnium case whereas the yield of ions is very low in the tungsten case. So far XF_5, where X stands for either Hf or W, has yielded the best results [84]. These two methods of suppression will together give a ^{182}W/^{180}Hf background of 1×10^{-10}, which allows for a ^{182}Hf/^{180}Hf detection limit of 1×10^{-11}. Consequently there is at least two orders more suppression of tungsten needed. Winkler *et al.* have used the 14 MV tandem accelerator at Australian National University to developed a detection method that measures the energy loss of the ions in their +12 state when passing through mylar foils in front of the detectors. They achieve a small separation and with an appropriate cut in the energy spectrum the detection limit could perhaps, even if the detection efficiency goes down, be enhanced by two orders of magnitude [82]. However, it would be a huge advance if the interfering isobar could be removed already before the injection into the tandem accelerator, i.e. on the low energy negative ion side. Using the production yield from the ion source as an estimate of the relative magnitudes of the two molecule's electron affinities, the situation seems to be favorable for using a laser suppressing scheme but the exact values of their electron affinities are unknown. Results from the search for these molecular quantities are presented in the results section 7.3.3 and in paper **IX**.

[3]This is not 100 percent true for lighter ions where it is possible to measure differences in energy loss when the particles are passing through matter [83]. In the case of ^{36}Cl analysis for example, this method suppresses ^{36}S by a factor of about 200. However, these methods are usually not as effective for heavier ions.

6 Experimental Setup

All experiments in this thesis are laser photodetachment experiments and they all employ the detection of the residual neutrals to investigate the process. Papers **I**, **II**, **IV**, **VII**, **VIII** and **IX** were performed at the negative ion spectrometer GUNILLA[1] in Gothenburg. The three experiments presented in paper **V** and **VI** were performed at the CRYRING storage ring at the Manne Siegbahn Laboratory in Stockholm. The experiments at Denison University, Granville, Ohio, USA led to paper **III**. Finally the experiment described in paper **X** was conducted at Oak Ridge National Lab, Tennessee, USA. These apparatuses all consist of an ion source, a mass selecting magnet, focusing and steering ion optics, an interaction region and a particle detector. All the systems are linear accelerators except CRYRING which is a storage ring.

6.1 System Parts

6.1.1 Sputter Ion Sources

Cesium sputter sources have been used since V. E. Khrohn in 1968 discovered that the yields of negative ions could be highly increased in the presence of a group 1 metal [85]. The coaxial cesium sputter source was developed in 1973 by Middleton [86], who also provided recipes for suitable materials to use as cathodes when producing a specific negative ion: The Negative Ion Cookbook [87]. Some refinement was carried out by G. D. Alton during the 1980's [88, 89]. Of the sputter sources used in the experiments described in this thesis, three are from commercial vendors and one is home built, but they are all based on the same principles.

Figure 6.1 shows a drawing of a coaxial negative ion cesium sputter source and the insert shows the principle of the sputtering process. Cesium is evaporated in an oven and is sprayed via a feed tube onto a helical or spherical heat ionizer. The Cesium atoms are thermally ionized and accelerated by an electric field of a few kV towards the cathode.

[1] The acronym stands for: Göteborg University Negative-Ion Laser LAboratory.

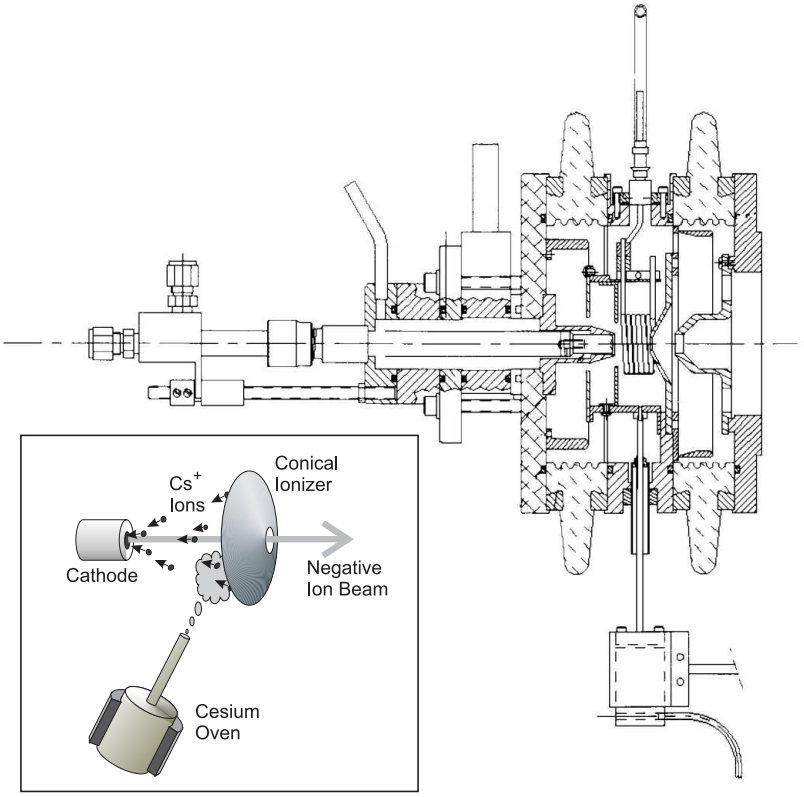

Figure 6.1: A drawing of a coaxial negative ion cesium sputter source. The insert is a principal sketch of the sputtering process. The source is negatively biased on 3 - 10 kV and the cathode is on a potential 1 - 4 kV with respect to the ionizer.

The cathode is a metal cylinder, usually copper or aluminium, that has a hole into which a suitable material that contains the element of interest can be placed. The cathode material has to be thermally and electrically conductive so that no heat or charge build up occurs during the sputter process. Insulating material can be mixed with a metal powder to provide conductance. When the cesium ions hit the cathode material they will sputter fragments of the cathode material but they will also form a thin Cs-layer on the cathode's surface. The presence of Cs will lower the work function of the surface, making the donation of electrons to the sputtered fragments more likely [90]. Those fragments that acquire an extra electron will be accelerated back towards the cesium ionizer by the same electric field that accelerated the Cs^+-ions. The negative ion beam can be extracted from a hole in the ionizer and further accelerated.

6.1.2 Mass Selecting Magnet

The negative ion beam extracted from the sputter source consists of a variety of atoms and molecules. It is necessary to be able to study just one of these without the interference of the others. All sputtered fragments with the same charge are accelerated to the same kinetic energy but since their mass differs they will have different momenta. Particles with different momenta will follow diverging paths in a magnetic field. This makes it possible to utilize a dipole magnet as a mass spectrometer when slits are put at the object and image point of the magnet as depicted in Fig. 6.2. Depending on the construction of the magnet the focusing can be in one or two dimensions, so that the slits may be replaced with apertures in the case of two dimensional focusing. The

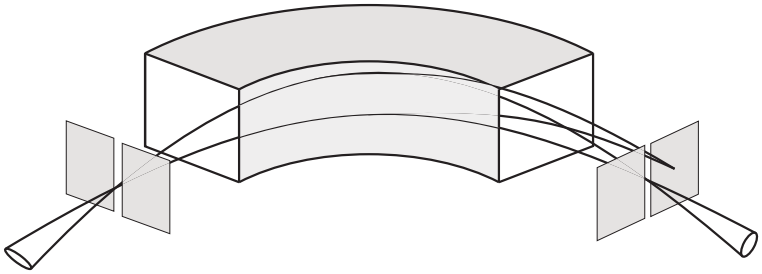

Figure 6.2: A schematic drawing of a single focus 90° sector magnet with slits at the object and image point. The mass following the central trajectory of the magnet will go through the image slit, while other masses will follow different trajectories and miss the slit.

second slit cuts away the dispersed images of masses with other trajectories than the central trajectory. The effect of bending in a dipole magnet is given by equilibrium of the centripetal and the Lorenz forces:

$$\frac{mv^2}{\rho} = qv\mathbf{B}. \tag{6.1}$$

Here ρ is the radius of the central trajectory through the magnet and $\mathbf{B}$ is the applied magnetic field. Eq. 6.1 can be transformed into a useful quantity called the bending power of the magnetic field:

$$mE_k = \frac{1}{2}(\rho q\mathbf{B})^2 \tag{6.2}$$

The mass resolution is often defined as $m/\Delta m$ where Δm is the full-with half-max of the mass peak at mass m. With 1 mm slits, the magnet at the university of Gothenburg facility GUNILLA has a theoretical mass resolution of $\frac{m}{\Delta m} = 500$.

6.1.3 Lasers

To perform a Laser Photodetachment Threshold experiment it is necessary to vary the photon energy. This can be done with a fixed frequency laser by Doppler tuning the photons in the ions rest frame, i.e. varying the acceleration voltage of the ion beam [91] or by changing θ [92, 93]. The more common way, however, is to use a tunable laser system.

A large part of the existing results from LPTS experiments have been produced using dye-lasers. Dye lasers was also used as the light sources in papers **III**,**V**,**VI** and **VII**. Dye lasers use a dye in solution to convert a pump laser pulse to a laser pulse of a desired photon energy. A planar jet of the dye-solution is sprayed at the Brewster angle from a slit nozzle through a laser cavity and is pumped by the focused radiation from a single frequency laser. The dye exhibits a quasi-continuous number of lasing states over a wide, but limited, wavelength region. The specific output radiation is tuned in the cavity by an adjustable grating. The dye is collected and reused after passing through the cavity. When shifting to a different wavelength region the dye has to be exchanged. With the development of optical parametric converters, explained next, the more labor- and chemical consuming dye lasers will probably be phased out.

Tunable radiation over a wide energy range can be provided by optical parametric converters. The three photon optical parametric process involves the annihilation of one photon and the creation of two new photons. The higher energy photon of the two is generally called "the signal" while the lower energy photon is dubbed "the idler"[2]. The incoming, annihilating, wave must be supplied by a pump laser in order to achieve an effective and useful conversion. The conditions for this process are that the energy and momentum of the interacting photons must be conserved according to the expressions:

$$\begin{aligned} \omega_{pump} &= \omega_{signal} + \omega_{idler} \\ \mathbf{k_{pump}} &= \mathbf{k_{signal}} + \mathbf{k_{idler}}. \end{aligned} \tag{6.3}$$

Due to the normal dispersion in an optical medium the second equation, the momentum conservation, or phase matching condition, cannot be satisfied: the k-vector of the pump is always too long to match the sum of the k-vectors of signal and idler waves. An optical parametric converter uses the nonlinear optical properties of birefringent crystals, usually BBO (BaB_2O_4) or KTP ($KTiOPO_4$ or Potassium Titanium Oxide Phosphate), to

[2]To be specific, using the terminology originally adopted for microwave technology, the "signal wave" is the wave that is being amplified while the "idler wave" is the difference frequency that is generated as a byproduct.

compensate for the material dispersion. Depending on the angle of the incoming wave with respect to the optical axis there is always a specific pair of signal and idler waves that will match up the k-vector of the pump wave. Tunability then is obtained by rotating the crystal relative to the direction of propagation of the pump wave so that the pair of matching signal and idler waves have to change in frequency and momentum. The parametric process is more likely to occur if a ω_{signal} or ω_{idler} photon is present, in similar manner to the stimulated emission process in ordinary lasers. Placing the crystal inside a optical cavity therefore creates an Optical Parametric Oscillator (OPO). The parametric process is a single three photon transition and therefore has a small cross section resulting in a high threshold for oscillation for the OPO. This means that the OPO has to be pumped by quite high powers, but once above the threshold the conversion is very effective. The bandwidth of the OPO is determined primarily by the bandwidth of the pump, the angular divergence of the pump beam, and the crystal length[3] [94]. The tuning range is in principle defined by the photon energy of the pump and the optical transmission properties of the crystal material, but is in general much wider than in any other tunable laser radiation source. When a strong down-converted beam is established from the OPO it can be followed by a second optical parametric converter for amplification. This will by definition also create an amplified beam of the matching wave according to the conditions given in 6.3. This step is called an Optical Parametric Amplifier (OPA).

6.2 GUNILLA

The small mass spectrometer/collinear laser photodetachment threshold spectroscope GUNILLA at the Department of Physics in Göteborg (Fig. 6.3) has recently been upgraded to achieve better mass resolution and higher transmission. Several of the experiments in this thesis were performed with the older version of the apparatus but the present state of the machine will be the one described here.

The ions are produced in a commercial Peabody Scientific negative ion cesium sputter source, accelerated and focused in the x-direction by a one dimensional lens onto the variable one dimensional entrance slit in front of the 90° bending magnet. The focus is imaged by the magnet at the variable, in both x- and y-direction, exit slits. The y-direction is focused by an einzel lens prior to the entrance slits to the middle of the magnet and refocused again by a one dimensional lens to the exit slits. This arrangement maximizes the transmission through the magnet which only has focusing properties in the x-direction. Directly after the exit slits a Faraday cup can be inserted for diagnostic purposes. After the exit slits the beam is focused again by an electrostatic quadrupole triplet (QT). A beam profile monitor is placed immediately after the QT for further di-

[3] Absolute phase matching is in principle only required for an infinitely long crystal.

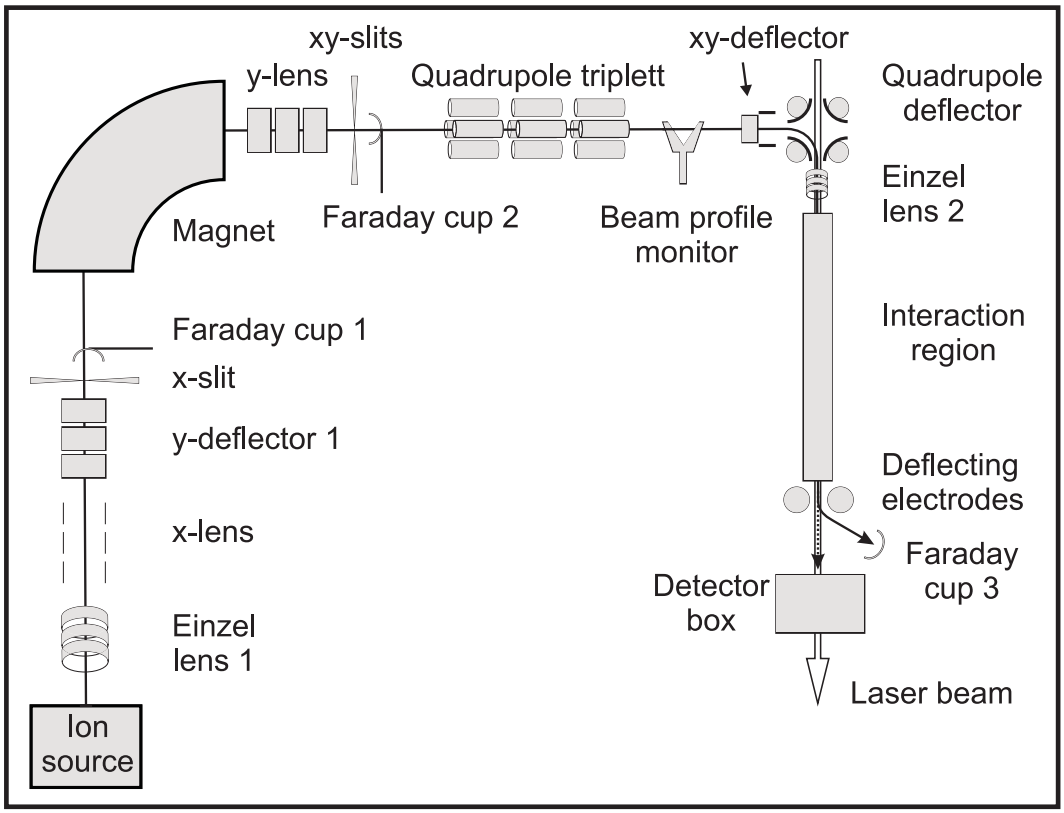

Figure 6.3: A schematic drawing of the ion beam apparatus at the University of Gothenburg.

agnostics of the beam. The beam can then be steered by x- and y-deflectors before being brought into the bending electrostatic quadrupole deflector. Here the beam is bent into the interaction region, which is preceded by an additional einzel lens, then defined by two 3 mm apertures situated 61 cm apart. The ion beam is then bent into a Faraday cup by two cylindrical electrodes placed after the interaction region while neutrals continue into the neutral particle detector.

A detailed description of the neutral particle detector can be found in [95] but its main features will be outlined here. Secondary electrons are produced by the neutrals in collision with a glass plate coated with tin-doped Indium-oxide (In_2O_3:Sn). These electrons are guided by a positive potential (150 V) towards the entrance of a Channeltron Electron Multiplier (CEM). The whole arrangement is placed in a housing biased at -50 V to prevent stray electrons from entering the detector. When the laser light strikes the glass plate a very large number of photo-electrons that can saturate the CEM is produced. These electrons are prevented from reaching the CEM by means of a mesh, connected to a fast triggered switch, placed between the glass plate and the CEM opening. During

the laser pulse the mesh has a potential of -70 V and will thus repel the electrons caused by the light. Since there is a finite flight time for particles from the interaction region to the detector it is possible to then switch the mesh to -30 V in time for the arrival of the photodetached neutrals (Fig. 6.4). Reflections from the glass plate exit the housing through holes in the walls. The signal produced by the neutral particle detector is

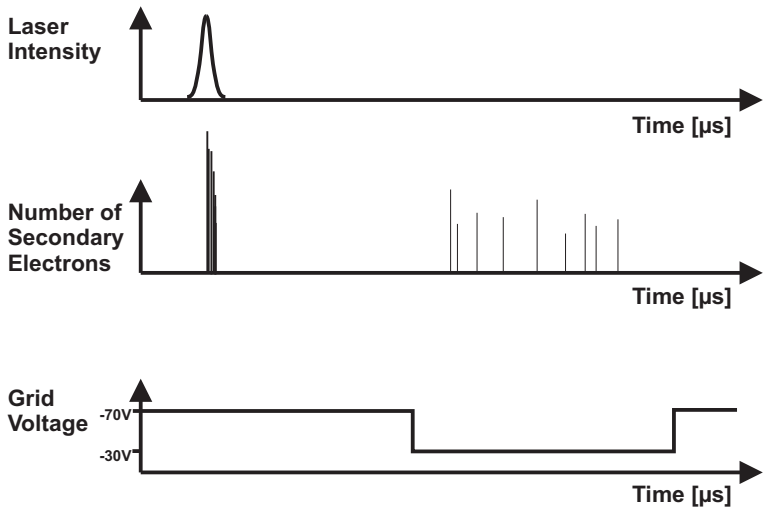

Figure 6.4: To prevent photo electrons from entering the CEM, a switchable mesh, timed to coincide with the arrival of the neutrals produced by photodetachment, is mounted in front of the CEM.

amplified and sent to a fast gated counter with a built in discriminator. The CEM has a maximum count rate in ”burst mode” of about 1 MHz. At higher pulse densities the CEM will gradually discharge and the amplitude of the pulses from the CEM will start to decrease so that, at some stage, they will be too small to be detected. The counter is trigged by the laser light via a photo diode and a delayed gate enables counting only during the time that the photodetached neutrals arrive at the detector. For an LPTS measurement, the signal counted by the gated counter, the ion current, and the wavelength and energy for each laser pulse is recorded by a `LabView`-program. A continuously updated signal is displayed by the program but normalization is done separately during the manual analysis of the data.

The two optical parametric converters at Gothenburg that provide the laser radiation for the experiments use tripled- or a combination of doubled- and fundamental photons from two 10 Hz Nd:Yag lasers. The combined laser systems have a continuous tuning range from 5000 nm to 220 nm or equivalently from 0.25 to 5.6 eV. The energy of each laser pulse is measured after passing through the interaction region. The wavelength of each pulse is measured with a wavelength meter. The wavelength meter also measures the pump photon frequency every 100 shot to monitor longtime drifts in the pump laser.

The rest of the time the unused branch of the split photons is measured and the applied radiation's frequency is calculated from

$$E_{\gamma}^{applied} = E_{\gamma}^{pump} - E_{\gamma}^{unused}. \tag{6.5}$$

The ion source is evacuated by a diffusion pump while the rest of the system is pumped by one turbo pump and several ion pumps. The apparatus is differentially pumped using apertures placed after the ion source and at the entrance to the interaction region. The pressure in the interaction region is on the order of 10^{-9} mBar.

6.3 Denison University

The apparatus at Denison University, Granville, Ohio, US (Fig. 6.5) was constructed as a small crossed beam laser photodetachment spectrometer during my visit there in the spring/summer of 2004. I constructed and mounted some of the ion beam optics that were used during the first experiment. The description here refers to the version of the machine used during the initial experiments leading to paper **III**.

The ions are produced in a commercial SNICS sputter source. Ions are accelerated, deflected if necessary, and focused on an aperture at the focal point of the doubly focusing magnet. This aperture also functions as a differential pumping aperture. In front of this aperture a beam profile monitor is situated. The focus at the entrance aperture is imaged at the exit focal point of the magnet where another aperture is placed. This aperture is mounted on a movable arm so that two sizes can be chosen leading to either low resolution with high transmission or higher resolution with lower transmission. A second beam profile monitor is placed after the exit aperture to provide real-time information of the beam shape and position. The beam travels through x and y deflectors before entering the experimental chamber. Here it goes through a y-displacement, to remove background neutrals created by rest-gas collisions during the transport, before being perpendicularly intercepted by the focused laser beam. The ion beam is deflected into a Faraday cup while the neutrals impinge on a dynode chain. The background is further kept as low as possible due to the very low pressure ($\sim 10^{-9}$ mBar) in the interaction chamber. The dynode chain is run in analogue mode and the voltage output is recorded by a digital storage oscilloscope.

The optical parametric converter providing the laser radiation is seeded by a narrow-banded dye laser and pumped by the doubled fundamental from a Nd:YAG at 50 Hz. The wavelength of the light is measured with a wavelength meter.

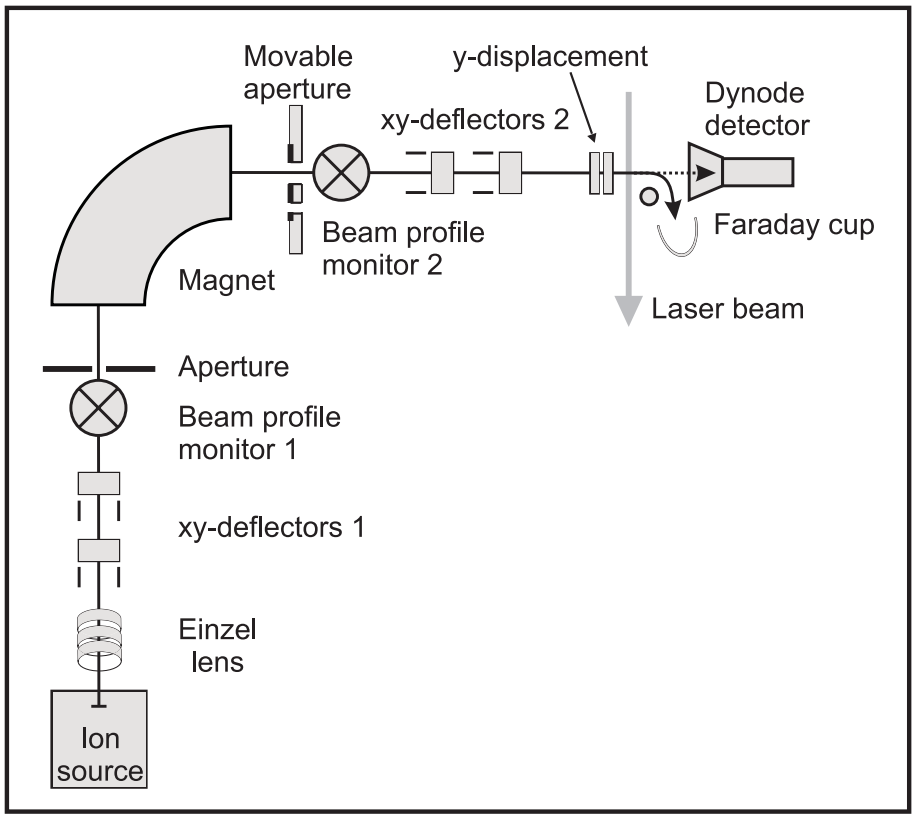

Figure 6.5: A schematic drawing of the ion beam apparatus at Denison University.

6.4 Manne Sighbahn Laboratory

The magnetic storage ring CRYRING at the Manne Siegbahn Laboratory was initially built to study highly charged ions produced in a cryogenic electron beam source called CRYSIS and was hence named CRY-RING. The storage ring has proven to be a useful device not only for highly charged ions, but also for experiments on both atomic and molecular ions, positive as well as negative, that have been conducted throughout the years. CRYRING is a ring type accelerator used for investigating ions during much longer times than what is often possible in a linear accelerator. The experimental facilities consist of a variety of ion sources, the injection beam line and the storage ring itself, made from 12 straight sections and 12 thirty degree bending magnets (Fig. 6.6). The ring has a circumference of 51.6 m. With its electron cooler CRYRING is an excellent facility to perform high-resolution electron-anion collision experiments [96, 97] and CRYRING has also been used to study the long lifetimes of excited states in positive ions such as Ti^+ and Fe^+. [98, 99]

After extraction from the sputter source the ion beam is accelerated to 40 keV and then magnetically mass-selected. The beam passes through a radio frequency quadrupole accelerator, which, for the experiments presented in this thesis, is used only for focusing purposes, before it is injected into the ring. Injection is completed after the first ions have made about ten turns. A radio frequency accelerator in the ring is used to accelerate the injected ions to the desired energy. The storage time of the ions depends on their destruction rate by collisions with background gases. Therefore, the vacuum is kept as low as possible and the ring usually has a working pressure below 10^{-11} mbar. A rigorous description of the characteristics of the stored ion beam can be found in the thesis *Beam Dynamics and Injection in CRYRING* by A. Simonsson [100]. The interaction region for laser detachment experiments is placed in one of the straight sections of the ring, with the detector mounted in the tangential direction after one of the bending magnets. A neutral particle detector, such as the one described in section 6.2, is mounted at

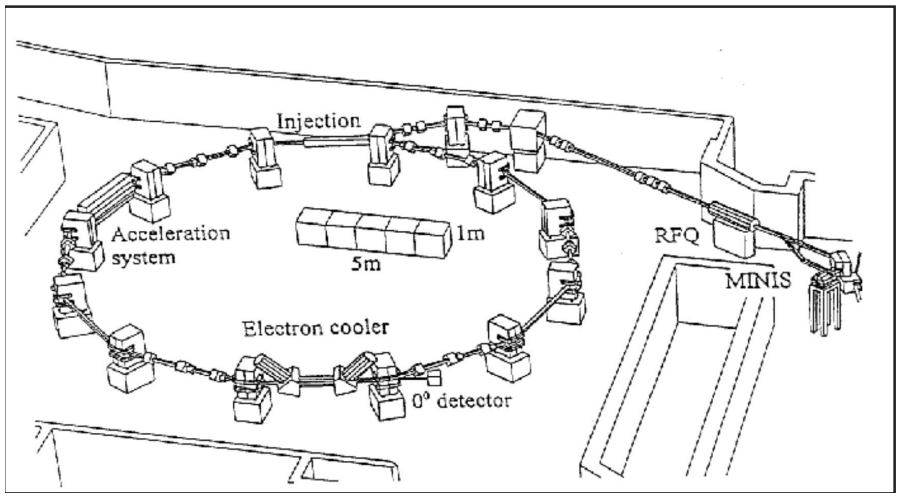

Figure 6.6: A schematic drawing of the ion storage ring CRYRING. The sputter ion source is installed at the MINIS injection beam line.

the end of the tangential beamline and the amplified signal is recorded by a computer system. A more thorough description of the data acquisition system used in paper **V** is given in the result section.

Laser light is brought by an optical beamline consisting of suitable mirrors, prisms and lenses into the interaction region via a vacuum window.

6.5 Oak Ridge National Lab

The experimental setup at Oak Ridge National Lab (ORNL) contains one specific component that has not been described earlier: The gas filled Radio Frequency quadrupole ion guide or the ion cooler. This device will be described here, after a brief description of the complete apparatus (Fig. 6.7).

The negative ions are produced in a cesium sputter source. Ions are accelerated and focused, then mass-selected in a 90° sector magnet with variable slits at the image point. The mass-selected ion-beam is decelerated, guided through the ion cooler and then re-accelerated. The beam is bent 90° in an electrostatic quadrupole deflector into

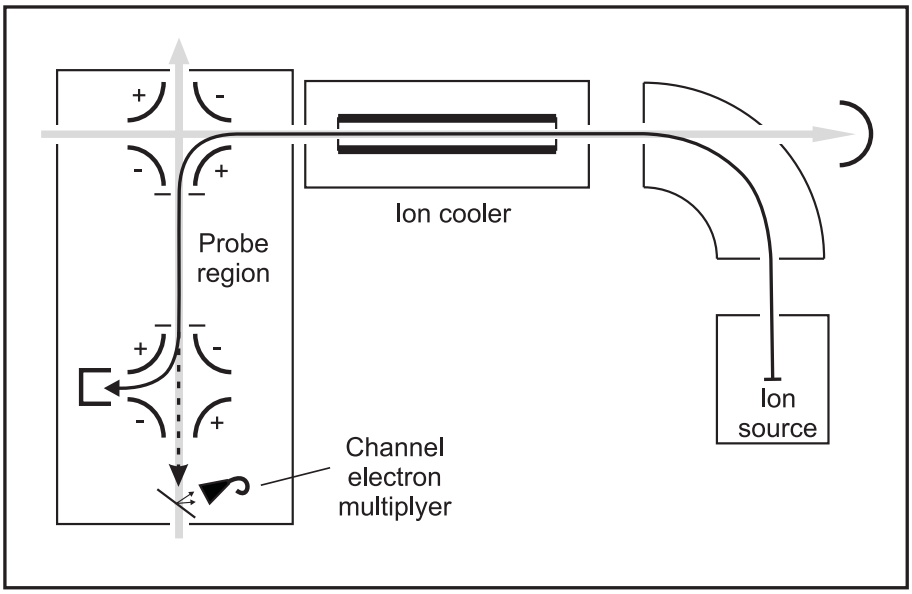

Figure 6.7: A schematic drawing of the experimental setup at Oak Ridge National Lab.

a collinear laser interaction region. At the end of the interaction region the ion beam is bent into a Faraday cup while neutrals continue on towards a neutral particle detector of the same kind as described in section 6.2. The signal from the detector is amplified and recorded by a computer using a Multi-Channel Scalar Card. Laser interaction can also be provided collinear in the ion cooler via two vacuum windows, one at each end of the ion-beam-transport leg between the magnet and the electrostatic quadrupole deflector. The laser power through the ion cooler is measured after passing through this leg and represents only a relative value. The value before entering the chamber must also be measured as a reference. The probe laser power is measured after passing through the chamber containing the collinear probing region.

During the experiment described in paper **X** two Nd:YAG lasers were used. One provided the radiation through the ion cooler. This laser operated at a maximum rate of 20 kHz. The other operated at 20 Hz and provided the probe pulse applied in the interaction region after the electrostatic quadrupole deflector.

The Ion Cooler

The concept of the ion-cooler was first developed for use with positive ions. The beam is decelerated to a suitable energy for injection into a Radio Frequency (RF) quadrupole situated inside a buffer gas cell filled with helium. The transition to the much more fragile negative ions demands that the ions are decelerated before they enter the buffer gas to avoid neutralization from collision with the helium atoms. While passing through the helium and being confined within the RF quadrupole field the ions lose their axial and transverse energy to the buffer gas. The ions are eventually thermalized and drift along the axis of the quadrupole either by diffusion or guided by a weak electrostatic field. At the exit of the RF quadrupole they are re-accelerated to their initial energy again with the energy spread from the sputter source removed.

The quadrupole consists of four parallel rods equally spaced on an inscribed circle with a radius r_0. A description of the essential characteristic of a RF quadrupole can be found in the article *Collisional cooling of negative ion-beams* [78] by Y. Liu *et al.* Under certain conditions the movements of the ions in the quadrupole can be approximated with movements within a simple pseudo-potential. Provided that the displacement of an ion during one RF cycle is small compared to its distance from the quadrupole axis, the time-averaged effect of the oscillating RF field will cause the ions to move as if they were confined in a parabolic potential well, Ψ, given by

$$\Psi(r) = \frac{eV_{rf}^2 r^2}{m\omega^2 r_0^4}. \tag{6.6}$$

Here V_{rf} and ω is the amplitude and the angular frequency of the RF voltage, and m is the mass of the ion. This means that the ions undergo slow harmonic oscillations around the quadrupole axis as they travels through the ion cooler. If the ions experience repeated collisions with atoms of much lighter mass, their kinetic energy in all three degrees of freedom will be redistributed among the colliding atoms. This is known as collisional cooling and is achieved in the ion cooler by filling the quadrupole with He gas at a pressure of approximately 10^{-5} mBar. The cooling of the ions transverse energies also damps the harmonic oscillations such that the ions will be confined at the lower regions of the potential well described in Eq. 6.6, i. e. close to the axis of the quadrupole.

The ion cooler at ORNL (Fig. 6.8) is constructed with four, 8 mm diameter and 40 cm long, cylindrical RF quadrupole rods, equally spaced on an inscribed circle with a radius of 3.5 mm between electrode surfaces. It also has four electrode rods tapered at a very small angle in the z-direction placed between the RF rods. These creates a small DC field along the z-axis that guide the ions slowly through the quadrupole. At the entrance the ions are focused through a 3 mm diameter aperture and after being guided through the cooler they exit through a 2mm diameter aperture. The quadrupole is placed in a housing enclosed by the entrance and exit apertures with 1mm gaps, so that buffer gas let into the housing can only escape through the entrance and exit apertures and the 1mm gap where it is pumped away by a turbo pump. At the entrance, as well as at the exit of the RF quadrupole, electrode systems are mounted. The entrance system is used to decelerate the ion beam to very low energies (<50 eV) and to focus the beam onto the 3 mm diameter aperture. The exit system re-accelerates the cooled ion beam to its initial energy. The main source of beam loss through the ion cooler is due to collisions with escaped buffer gas in the deceleration and acceleration regions. Here the energy in the collisions is high enough to detach the negative ions. To minimize this, turbo pumps are placed at both electrode systems. A detailed description of the cooling characteristics and the ion guide is given in *A high efficiency RF quadrupole ion beam cooler for negative ions* [101]by Y. Liu *et al.*

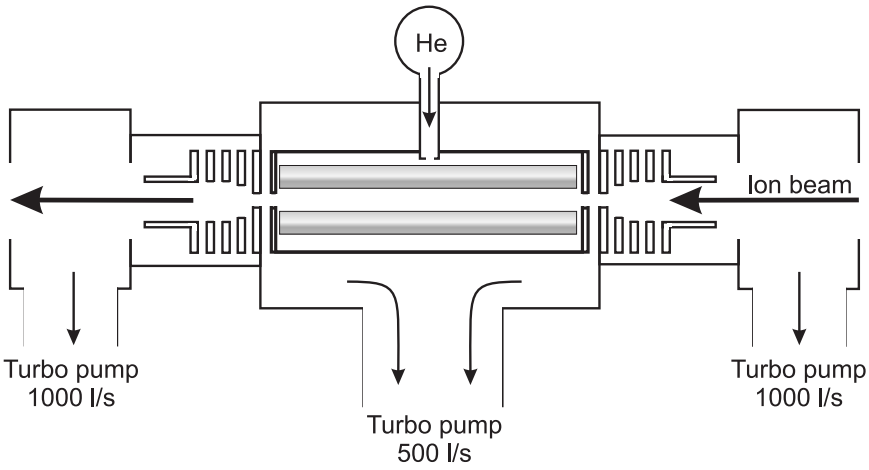

Figure 6.8: A schematic drawing of the ion cooler at Oak Ridge National Lab.

7 Results

7.1 Structure

These experiments are performed to search for detailed information of the binding energies and excited states of negative ions. They aim to be as precise as possible and to reveal new structural features, such as excited states or resonant phenomena in the cross sections. Three out of the four experiments of this type were performed at the university of Gothenburg, while the Ce^- experiment was performed at Denison University.

7.1.1 Paper I : The electron affinity of phosphorus.

In Paper I we report on a measurement on the electron affinity of phosphorous using laser photodetachment threshold spectroscopy at the collinear laser- ion beam spectrometer in Gothenburg. The total cross section consists of three superimposed s-wave thresholds. Each threshold represents the opening of the photodetachment channel from a fine structure component of the ^3P_J ground state of the negative ion. In order of increasing photodetachment energy they correspond to the excited levels $^3P_0$, $^3P_1$ and the $^3P_2$ ground state level, respectively. The background below the $^3P_0$ state is essentially zero allowing for a very precise determination of the photodetachment threshold. The induced Doppler shift caused by the collinear geometry is corrected for by acquiring threshold values for both parallel and anti parallel laser- ion beams and then using Eq. 4.4 to extract the Doppler free value. The pulsed laser was scanned over the region of interest and the number of neutralized atoms, the laser power through the apparatus and the laser frequency were recorded for each laser shot. This was important since the output of the OPO/OPA producing the laser light has a rather large pulse to pulse photon energy variation. The single shot bandwidth was about 0.2 cm^{-1}, which was the limiting factor in the accuracy of the experiment. The accuracy of the wavelength meter was controlled against four well known Rb lines in a Doppler free saturation spectroscopy setup. The Doppler free threshold wave numbers acquired are 5758.4(2), 5841.0(2) and 6022.4(5) cm^{-1} for the $^3P_0$, $^3P_1$ and $^3P_2$ states, respectively. The result was compared with the two previous measurements by Feldmann [102] and Slater and

Lineberger [103]. Our result is consistent with the previous measurements but has an almost one order of magnitude smaller error, as can be seen in Fig. 7.1.

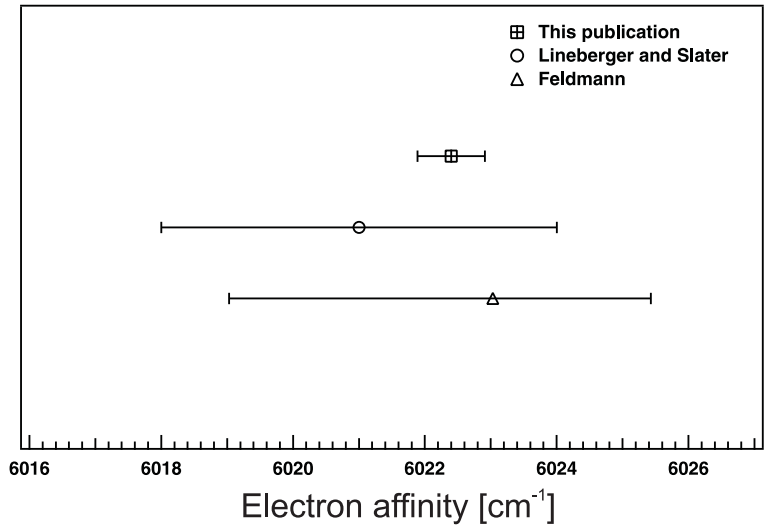

Figure 7.1: the electron affinity of phosphourus in a comparison between our measurement and the measurements of Feldmann and Slater and Lineberger

This experiment was initiated as a test of our data acquisition system, where all data is stored ”shot by shot”. After the acquisition the data is binned according to photon energy. The new acquisition system was motivated by the fact that our OPO/OPA would, on about every tenth pulse, give a pulse that would be several bandwidths away from the main frequency (see Fig. 7.2). If these pulses were not sorted and placed in their correct bin together with the accompanying data, they would have caused signal from the rapidly increasing s-wave cross section to appear below the actual threshold.

7.1.2 Paper II : The electron affinity of tungsten.

In paper II we report on a measurement of the electron affinity of tungsten using LPTS at the University of Gothenburg. The experiment is performed with the same technique as described in paper I. The result is a total photodetachment cross section where the p-wave threshold in Fig 7.3 corresponds to the opening of the $^6S_{5/2}$ ground state photodetachment channel of the $^{182}W^-$-ion.

The electron affinity was measured to be 6583.6(6)cm^{-1}. The uncertainty of 0.6 cm^{-1} is about two orders of magnitude better than the previous results from Feigerle *et al.* [104] and Bengali *et al.*[105]. We also measure a non-zero background from photodetachment signal at energies below the threshold. Such signals could in principal stem

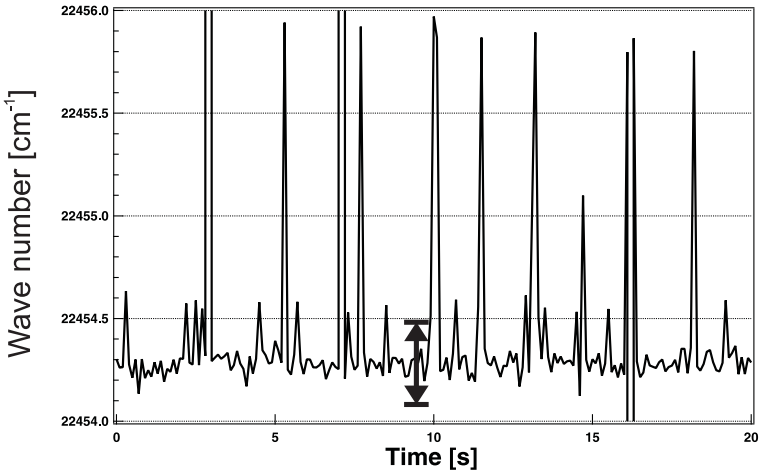

Figure 7.2: The wavelengths of the pulses from the OPO/OPA detected by the wavelength meter over a time span of 20 seconds. The vertical bar indicates the single pulse bandwidth of the converter. The repetition rate of the laser is 10 Hz.

from three sources: An excited state, a contaminant in the mass-selected beam, or contaminating photons of higher energy in the laser beam. According to previous data, the $5d^5 6s^2\ ^6S_{5/2}$ state should be the only bound state in W^-. The photodetachment data collection was preceded by a careful mass analysis of the ion beam to reveal any possible contaminants. We compared the mass spectrum with the natural isotopic abundance of tungsten with good agreement. We also looked for atomic ions that could combine to a molecule with mass 182 in a full length mass spectra. None of these checks showed any indications of contamination in the ion beam. When the signal beneath the threshold became apparent we also performed checks at the four major peaks in the mass spectra to verify that this non-zero background appeared in all peaks. This check revealed expected hydride contaminations in all mass peaks except the peak at mass 182 u but also confirmed the photodetachment signal seen below the ground state threshold energy. Finally we checked the laser beam for contaminants of unconverted 1064 nm pump-beam photons from the OPO/OPA. A weak component was found, but the signal did not decrease substantially when 90% of this was filtered out. Thus we are led to conclude that the photodetachment signal present beneath the threshold must originate from a previously unknown excited state in the tungsten negative ion. A search was initiated for the threshold for this detachment but only a lower limit was found. At 3500 nm the transmission of the laser beam through the vacuum windows mounted onto the spectrometer is too poor to be useful. These windows will however be replaced in the near future. Searching the literature for information about the structure of W^- only provides the two references stated above.

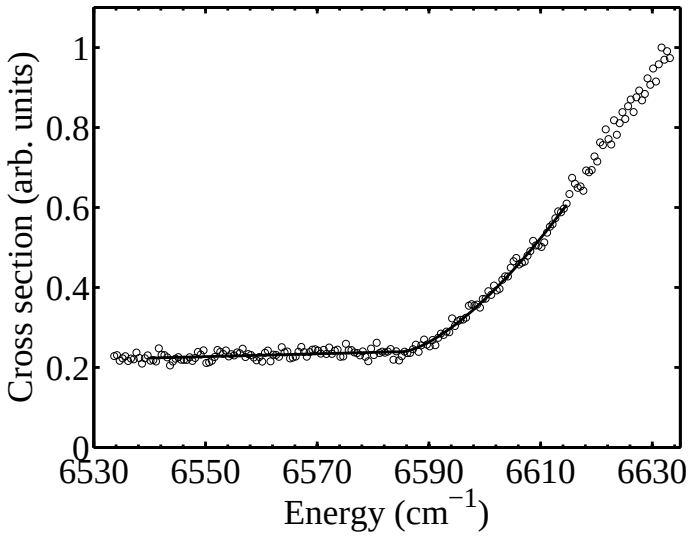

Figure 7.3: The relative photodetatchment cross section of tungsten

7.1.3 Paper III : Infrared photodetachment of Ce^-: Threshold spectroscopy and resonance structure.

In paper III a measurement of the electron affinity of cerium is reported. Along with the photodetachment p-wave threshold a series of resonances was also found in the total cross section, as illustrated in Fig. 7.4. Performing experiments on lanthanides is interesting since the presence of several open shells and the high number of electrons leads to strong correlation effects. The lanthanides are one of the least explored groups of elements when it comes to negative ions mainly due to the difficulties of producing strong and stable ion beams and that their electron affinities in general lie in the infrared photon energy range. In recent years the activity in the field has increased, in particular through the group of Thompson at the University of Nevada [106, 107].

The problem of producing a substantial and stable beam of cerium was solved by using a special cathode where the cerium powder was sealed by a tungsten cap in which a small hole was drilled. This prevents the cesium heat ionizer from being contaminated with the lanthanide [108], which otherwise would cause instability of the ion beam. In addition there will be tungsten sputtered from the cap, revitalizing the heat ionizer from any lanthanide contamination that nevertheless is occurring. In this way we could acquire a stable Ce^--beam throughout the whole experiment.

Cerium is the most extensively studied element of the lanthanides but the results for the electron affinity have been quite diverse, ranging from Thompson's value of 0.955

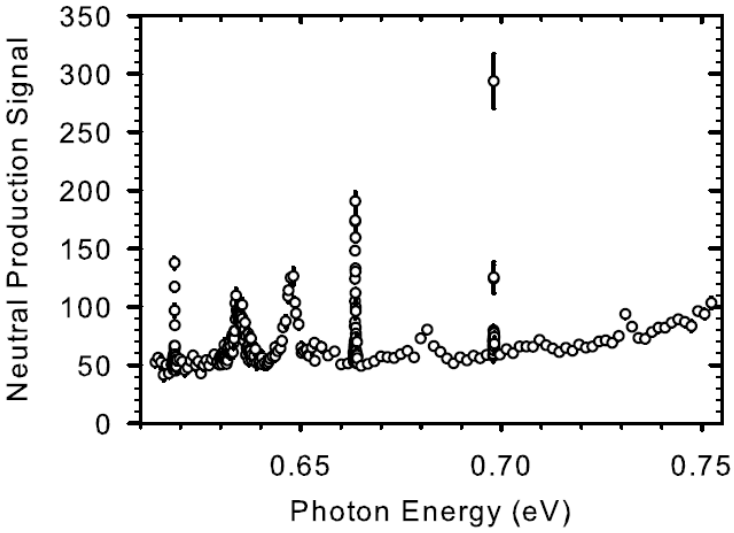

Figure 7.4: The relative photodetachment cross section of cerium with some of the resonances clearly visible.

[107] to a lower limit of 0.5 eV deduced from the yield of sputtered negative ions by Nadeau *et al.*[109]. Theoretical predictions have consequently favored lower values of the electron affinity. O'Malley and Beck even reinterpreted the electron spectroscopy data of Thompson *et al.*and extracted an electron affinity of 0.66 eV [35]. In an attempt to resolve this ambiguity we performed the first detailed laser photodetachment threshold spectroscopy experiment. The experiment revealed a rich spectrum of resonances which to some extent obscured the ground state threshold. Therefore a different approach in the fitting procedure has to be used, aided by the result from O'Malley and Beck. With the calculated electron affinity and a constant background level as fixed parameters, leaving the amplitude constant as the only free parameter in the initial fitting, the best possible fit was obtained. The fitting procedure was then repeated with different threshold values to determine the range of threshold energies that were consistent with the data. This fitting procedure yielded an electron affinity of 0.65(3) eV.

The spectrum of resonance structures seen in fig 7.4 could not be fully identified since their origin crucially depends on the position of the photodetachment threshold, for which the uncertainty encompasses all but one of the peaks. One interpretation of the data is that the three peaks lowest in energy, labeled A, B and C lie below the photodetachment threshold and may in that case be due to excited bound states of Ce^-. The signal measured at these peaks would then come from a two step detachment process where the first step is a resonant excitation from the ground state into an excited state of opposite parity. The second step is the photodetachment of this excited state. A similar process lead to the observation of the, up to now, only known bound excited state

of opposite parity in Os^- [53]. The calculations of O'Malley and Beck [35] predict three such states. An earlier calculation by Cao and Dolg [110] predicts two such states. However, peak B is strongly asymmetric, indicating a Fano-type resonance belonging to a state in the continuum. A resonance from a bound-bound dipole excitation has a lorenz profile, a criteria which is met by the resonance A. This is also the resonance lowest in energy i.e. the most likely to lie beneath the threshold. In this interpretation, cerium would be the second element in which a bound-bound state transition has been observed in a negative ion.

7.1.4 Paper IV : Observation of the $^2S_{1/2}$ metastable state in Pt^-.

In paper IV we present the first experimental observation of the $^2S_{1/2}$ excited state in the platinum negative ion. This state has been previously predicted in the calculations by Zollweg [111] and Thøgersen *et al.* [112] but has never before been observed experimentally. The state was observed by laser photodetachment threshold spectroscopy in Gothenburg and the acquired total cross section is illustrated i Fig. 7.5. The Doppler free threshold energy for photo detachment from the state corresponding to this p-wave cross section was measured to be 6851(13) cm^{-1}. To reveal possible isobaric contami-

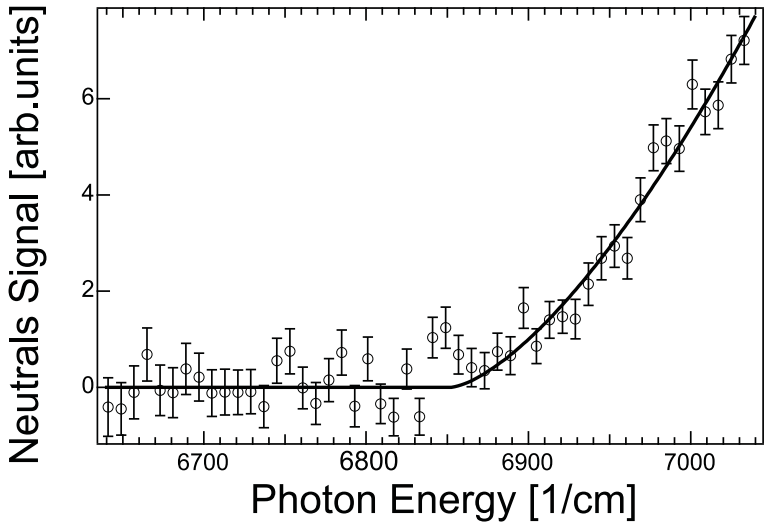

Figure 7.5: The photodetachment signal from the $^2S_{1/2}$ excited state in the platinum negative ion. Note that the signal below the threshold is zero, indicating that no further excited states are present.

nants in a mass-selected ion beam used for threshold measurements we have developed a method that we call a Laser Photodetachment Mass Scan (LPMS). The first step in order to determine if there are contaminants in our beam, is to acquire a mass spectrum

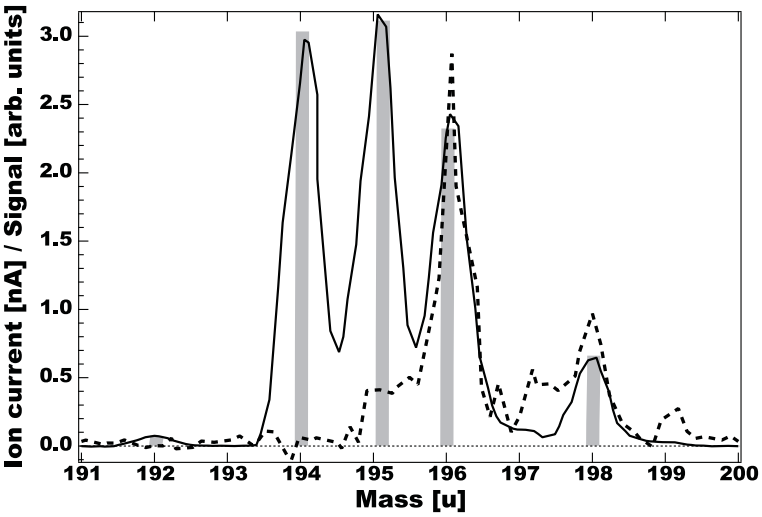

Figure 7.6: The ion current- and photodetachment mass scans of Pt $^-$. The current measured in the Faraday cup at the end of the system is represented by the solid line. The photodetachment signal acquired while scanning the magnet is represented by the dashed line. The natural isotopic abundance of platinum is illustrated by the grey bars in the figure

and compare this with the natural isotopic abundance. However, even if the isotopic ratio of an element, measured by the variation of the ion current in the Faraday cup while sweeping the magnetic field, seems to agree very accurately with the natural abundance, as is the case with the solid line in Fig. 7.6, trace amounts of a contamination with a low electron affinity can nevertheless give a substantial signal. If the energy of the laser radiation is below the photodetachment energy of the element under study, such a contamination would be the single source of signal. The laser photodetachment mass spectrometry is performed by applying the laser onto the ion beam and monitoring the neutral particle signal while sweeping the magnetic field. The resulting LPMS-spectra, with the laser wavelength a few cm^{-1}below the detachment limit for the proposed Pt^- state at 6851 cm^{-1}, can be seen represented by the dashed line in Fig. 7.6. While this spectrum in principle does not prove the absence of a contaminant with binding energies above the applied radiation, analysis clearly shows that all masses above 194 u are contaminated with species of negative ions that are not Pt^-. Masses 195, 197 and 199 show low signals that are most probably PtH^-, while masses 196 and 198 shows a stronger signal which we believe originates from CuCs ions[1]. Mass 194 u shows no signal at

[1]Both the masses and the isotopic abundance fit this suggestion. Cesium is always present due to the nature of the Cs sputter source and copper has been extensively used in the holder of the cathode material. During the experiment the platinum sample was mounted in an aluminum holder but small remains of copper in the interior of the source can not be ruled out.

all which proves that none of the observed LPMS-signals can originate from platinum, since all isotopes, disregarding a insignificantly small isotope shift, have the same binding energies. To further make sure that no contamination was present, a mass scan over the full mass range was performed, searching for components of a possible mass 194 u molecule, but no such elements were found. Thus it seems that the only uncontaminated peak is the one at mass 194 u and for this reason all data was attained at this mass.

That the signal in the threshold measurement could originate from photodetachment of excited states in the negative ion into excited states of the neutral was also considered, but is in principle ruled out by the zero background below 6850 cm^{-1}.

The negative platinum ion then has three bound states, where the $^2D_{5/2}$ ground state has a binding energy of 17 140(4) cm^{-1}[113]. The first excited state, the $^2D_{3/2}$ state, lies 9740.9(5) cm^{-1}above the ground state. This state has been measured to very high precision by Thøgersen *et al.* The $^2S_{1/2}$ level has been estimated by Zollweg to lie 12 847 cm^{-1}above the ground state while the Multi Configuration Dirac Hartree calculation of Thøgersen *et al.* predicted an excitation energy of 11 301 cm^{-1}. Our measured value for this excitation energy is 10 289(13) cm^{-1}. The calculations from Thøgersens group predicted the excitation of the $^2D_{3/2}$ state accurately within 205 cm^{-1}but there is a discrepancy between their prediction and our measured position for the $^2S_{1/2}$ state of more than 1000 cm^{-1}. Since the $5d^{10}s$ $^2S_{1/2}$ state has a different electron configuration than the ground state while the $5d^9s^2$ $^2D_{3/2}$ state is a fine structure component of the $5d^9s^2$ $^2D_{5/2}$ ground state with the same electron configuration, one might expect the calculation of the $^2S_{1/2}$ state to be more complicated.

To conclude, by careful analysis we have made sure that we use a pure Pt^- beam and that our only possible photodetachment channel is from the $^2S_{1/2}$ state into the continuum. Consequently we can state that we see the onset of photodetachment from the $^2S_{1/2}$ state in the negative Pt^- ion. Its binding energy is 6851(13)$cm^{-1}$and no further excited states exists above this state.

7.2 Dynamics

Excited states of negative ions are, as mentioned in the introduction, caused by term splitting or by fine structure components of the ground state. In almost all cases these states are of the same parity as the ion ground state. This means that, due to the quantum mechanical selection rules, radiative transitions to the ground state are forbidden. The absence of a discreet light emission spectrum thus makes traditional spectroscopy impossible and the method for measuring the lifetime of long lived states developed by Mannervik *et al.* [114, 115], measuring the decay of the prompt florescence from an

excited state in an ion storage ring, cannot be used. However, based on that method, but using the selectivity of photodetachment (see Fig. 7.7), we have developed a similar technique in which we are able to probe the population of an excited state at different times after the injection of ions in the storage ring. A controlled excitation into the desired state is not possible since the transition is ”forbidden” but the environment in the sputter source produces a non thermal distribution of different excited states. The probing of an excited state will show an exponential decrease of the population that approaches a steady state level where collisional excitation is balanced by radiative decay through M1 or E2 transitions. As the destruction of ions in the ring also generates an exponential decay of the total ion population, which affects the excited state proportionally, the final signal will be a double exponential. As an effect of this the upper limit of the lifetime measurable with the method is set when the two exponentials are approaching each other in decay time, making the determination of each specific exponential unreliable.

7.2.1 Paper V and VI : Radiative lifetimes of metastable states of negative ions.

In paper **V** and **VI** we report on a series of lifetime studies of metastable excited states in negative ions performed at the CRYRING heavy ion storage ring at the Manne Siegbahn laboratory in Stockholm. The experiments were performed on three different negative ions: tellurium, selenium and silicon. Their respective energy levels are shown in Fig. 7.7. The excited state was probed by a laser in the laser interaction section of the ring

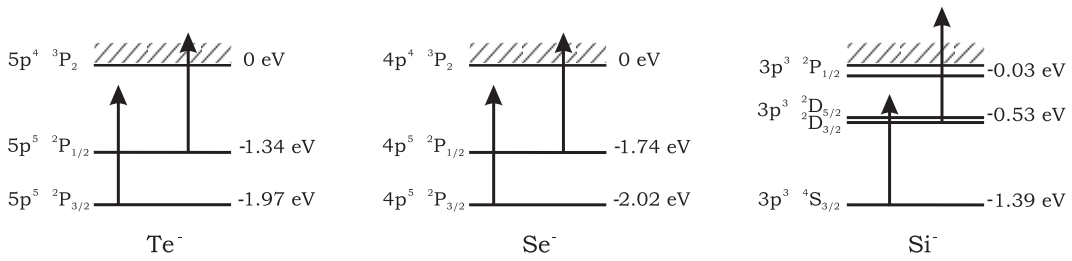

Figure 7.7: The level diagrams of the elements treated in paper IV. The excited state in Te^- and Se^- are fine-structure splittings while the excited levels in Si^- are term splittings. The $^2P_{1/2}$ state in Si^- is so weakly bound that it is assumed to be absent in the ion beam.

and the neutrals produced by the photodetachment process were detected. Since the measurement is destructive only one probe pulse per injection could be used. After the probing of the excited state the ions in the ring were dumped and the ring had to be refilled again for the next probe. For each new set of ions the 500 ns long probe pulse was shifted in time, where time zero was defined to be a few ms after the injection was

completed. To monitor the fraction of excited state ions and to be able to normalize the result with respect to the number of ions in the ring, a short probe pulse was applied at a constant time just after time zero and the result was compared with the background signal measured immediately afterwards. The background was also measured immediately before and after the moving probe pulse. The mean value of these two background measurements was then subtracted from the probe signal. A schematic presentation of the timing scheme is found in Fig. 7.8. A lower limit of the lifetime can be given by

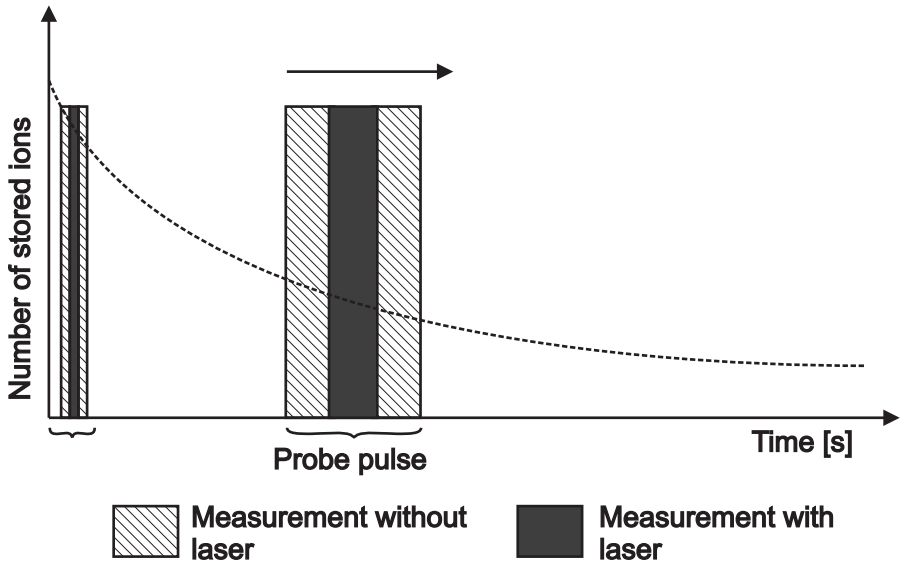

Figure 7.8: The timing of the system used to collect data in the lifetime measurement. The short normalization measurement is stationary while the probe pulse is moved forward in time between each injection of ions in the ring.

studying the decay of the excited state population when the laser is in continuous mode or when it is chopped at a low frequency during the whole ring cycle. The observed lifetime is, however, shortened because an additional depopulation mechanism is present in the form of the neutralizing laser. Data for Se^- using the moving pulse technique described above is shown in Fig. 7.9. Depopulation of the excited state by collision with background gas will also shorten the measured lifetime and the true radiative lifetime can only be found for zero pressure. Since that is not possible the second best alternative is to change the pressure in the ring and then extrapolate down to zero pressure. The data is then presented by using a so-called Stern-Vollmer plot (Fig. 7.10) where the intercept at zero pressure gives the radiative lifetime that would have been obtained at absolute vacuum. During these measurements the pressure was raised in one section of the ring by heating one of the vacuum pumps. The decay constant of the total number of ions in the ring was used as a measure of the pressure.

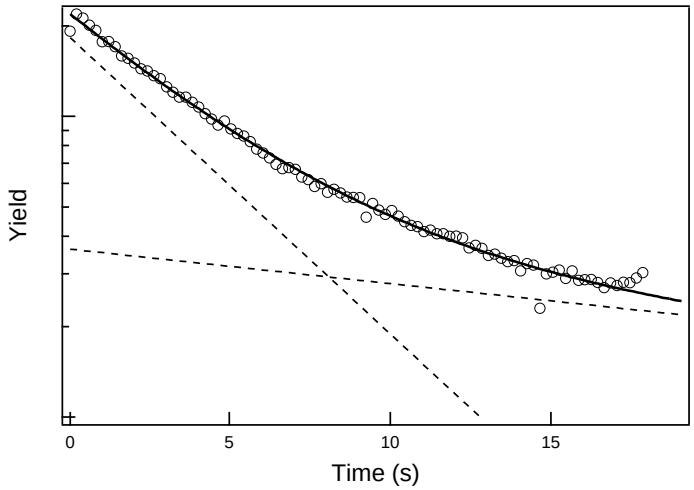

Figure 7.9: A semi-log plot showing the decay of the metastable $4p^5\ ^2P_{1/2}$ state in Se^-. Fits of the two exponential parts associated with the decay of the metastable state and the repopulation caused by collision are shown as dotted lines.

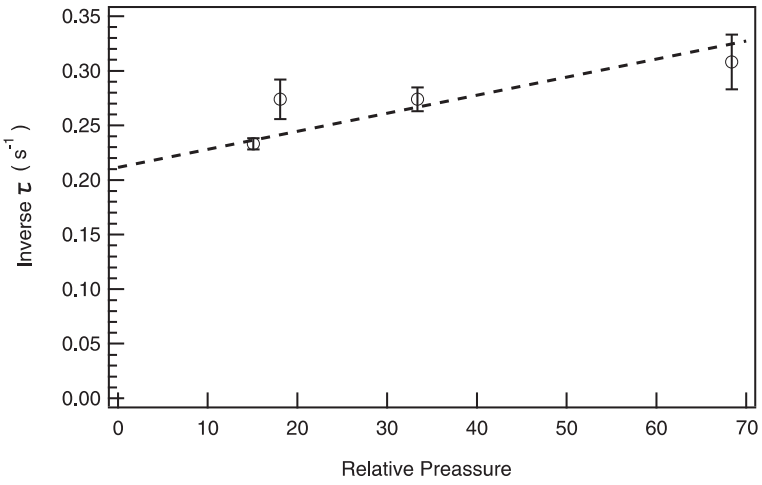

Figure 7.10: The Stern-Vollmer plot from the Se^- experiment. The lifetime of the excited state population was measured at four different relative pressures represented by the inverse τ from the exponential decay curve of the ions in the ring.

The result from the experiments corresponds very well to the theoretical values (Table 7.1) for all elements where a lifetime could be extracted. In the case of Si^- the lifetime of the excited state were close to, or exceeded the lifetime of the ions in the ring, and only a lower limit of the lifetime could be determined. This experiment was performed in collaboration with Charlotte Froese-Fischer. She used a Multi Configuration Dirac Hartree Fock calculation to obtain the theoretical lifetimes presented in table 7.1. The agreement between theoretical and experimental results is excellent and it should be noted that the measurements and calculations were done independently.

Table 7.1: The experimental and theoretical values for the lifetimes of the elements treated in paper **V** and **VI**.

Element	Transition	Measured Lifetime [s]	Calculated Lifetime
Se	$4p^5\ ^2P_{1/2}$-$4p^5\ ^2P_{3/2}$	4.7±0.7	4.92s
Te	$5p^5\ ^2P_{1/2}$-$5p^5\ ^2P_{3/2}$	0.42±0.05	0.454s
Si	$3p^3\ ^2D_{3/2,5/2}$-$3p^3\ ^4S_{3/2}$	>60	162s, 27.3h [116]

7.3 Applications

In this section four proof-of-principle experiments are presented, which demonstrate different ways in which laser light can be used to improve the purity of a mass-selected beam. Paper **VII** and **VIII** deals with isotopic contaminations while the last two are steps on the way to developing a method for the suppression of isobaric contamination.

7.3.1 Paper VII : Laser photodetachment mass spectrometry.

In paper **VII** we present a proof-of-principle experiment, showing how it is possible to employ the induced Doppler shift present in a collinear geometry between ion- and laser beam to achieve an isotope-selective detection. Since different isotopes have different mass they will have separate velocities when accelerated to the same kinetic energy. Thus, the Doppler shift will separate the thresholds of the different isotopes as they will experience different energies in the center of mass frame. If the laser is applied parallel to the ion beam the heavier, and therefore slower, isotope will start to photodetach at photon energies that the faster, lighter isotope will experience as an energy below the photodetachment threshold. The situation is illustrated in Fig. 7.11. If the energy separation between the two thresholds is made large enough to position a narrow bandwidth laser beam between them (position B in Fig. 7.11), we will have an isotope selective photodetachment process. Normally the separation of isotopes is not a problem. The problem arises when an ultra trace isotope is neighboring a stable isotope which can be many orders of magnitude more abundant. Since the sputter source is known to exhibit

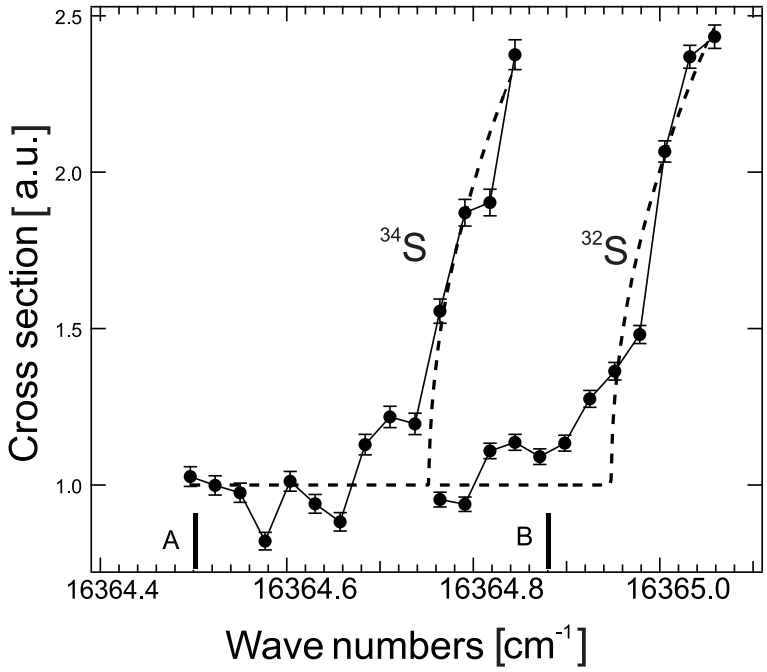

Figure 7.11: Due to the Doppler shift of the light experienced by the ions in a collinear geometry the thresholds for the different isotopes, ^{32}S and ^{34}S, will be separated.

a high energy tail in the atomic ion production, this tail of the highly abundant neighbor can extend to and overlap with the ultra trace isotope, causing severe contamination in the mass spectra.

The experiment was performed in Gothenburg and we show that isotope selective detection is possible to achieve at acceleration energies as low as 5 keV. By subtracting the signal acquired from a laser positioned at energy A, as indicated in Fig 7.11, from the signal acquired with the laser at energy position B we achieve the selective detection of ^{34}S. The signal acquired with the laser at point A consists of the collision background and a low amount of photodetached ions due to a weak but broadband laser radiation present in the output from the dye laser used for this experiment. The laser scheme shifted the detected isotopic ratio from the natural ^{32}S/^{34}S ratio of 23 to a ratio of about 0.5 or equivalently, suppressed the detection of ^{32}S by approximately 98%.

7.3.2 Paper VIII : Selective detection of ^{13}C by laser photodetachment mass spectrometry.

Paper **VIII** is a continuation of the selective detection using laser detachment in combination with the Doppler shift. The experiment was performed at the accelerator in

Gothenburg. This time, however, it is applied on two isotopes with a mass difference of one u: ^{12}C and ^{13}C. In addition to the technique used in paper **VII** we also used a second laser for depleting the beam from two weakly bound excited states in carbon [16] , which otherwise would have interfered with our measurement. The fundamental 1064 nm radiation from a pulsed Nd:YAG was sent counter propagating to the ion beam in the chamber prior to the bending of the beam into the interaction region. The depletion achieved with this setup was limited by difficulties in aligning the two beams for a maximum overlap. Nevertheless a substantial reduction of the background was reached, as illustrated in Fig. 7.12. This experiment was conducted using a prepared

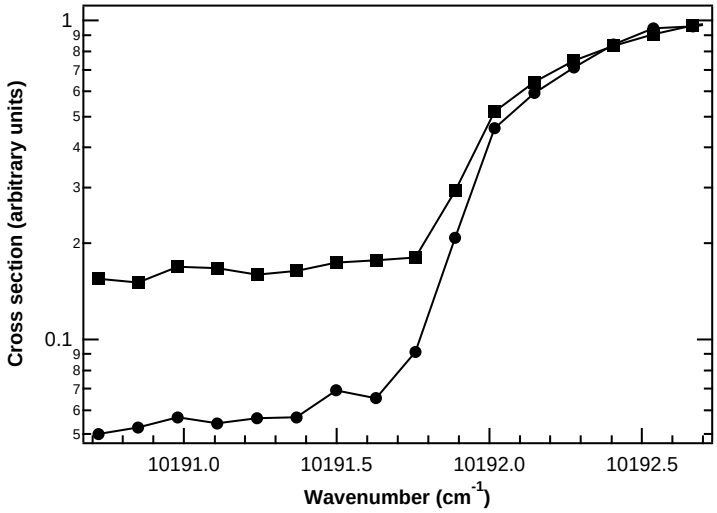

Figure 7.12: The background of photodetached ions from the two high lying excited $2D_{3/2,5/2}$ states (splitting is only 3 cm^{-1}) is removed from the beam by a 1064 nm laser beam before the ion beam is turned in to the interaction region. The squares represents the signal in the neutrals detector without using the clean-out laser, the circles show the background reduction of about 60% that was achieved with the laser on.

sample consisting of 50 % ^{12}C and 50 % ^{13}C. The result showed that we could reduce the detection of ^{12}C by more than 90 % as compared with the detection of ^{13}C.

7.3.3 Paper IX : A lower limit for ground state photodetachment of hafnium and tungsten penta-fluorides.

In paper IX we present an investigation into the onset of the ground state photodetachment of both HfF_5^- and WF_5^-. The background to this experiment is the search for ^{182}Hf which is in progress at the AMS laboratory at VERA in Vienna and explained in section 5.2. The search was performed in Gothenburg and the apparatus was upgraded to be

able to meet the demands on mass selection and transmission needed to be able to perform the experiment [117]. The mass spectra of the area around both molecules exhibits many different mass peaks belonging to various molecular ions. To disentangle the mass spectra and be able to find pure HfF_5 and WF_5 peaks the technique of Laser Photodetachment Mass Spectrometry had to be used. The situation is illustrated by Fig 7.13. When pure mass peaks were identified the photodetachment ratio between the two dif-

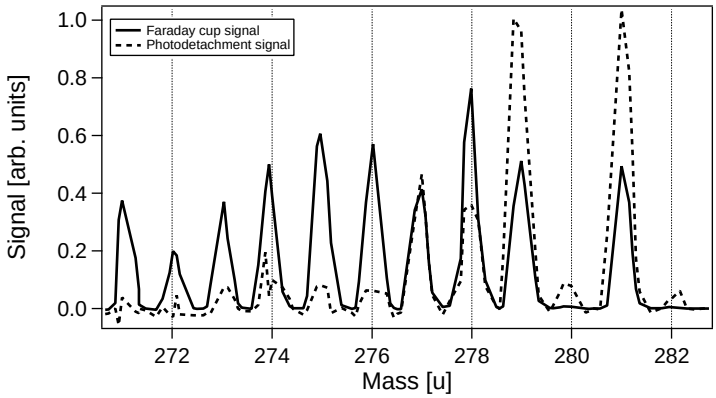

Figure 7.13: The photodeachment mass spectra (dashed line) from the region around WF_5^- plotted together with the corresponding ion current mass spectra (solid line) measured simultaneous in the last Faraday cup. Analyse of these spectra show us that the only clean peak of WF_5^- is the peak at 279 u. A similar analyse had to be done to find a pure HfW_5^- peak.

ferent molecules was measured at a few selected wavelengths. Both molecules showed a weak photodetachment signal in the range from 9400 - 28184 cm^{-1}. The ratio of photodetachment was constant within errors, with WF_5^- having approximately 1 order of magnitude higher cross section than HfF_5^-. An estimate of the absolute cross section gives roughly 10^{-20} cm^2 for WF_5^-. This is a small cross section and we draw the conclusion that the onset for photodetachment from the molecular ground state has not yet been reached. What we observe is most probably the detachment of excited state ions which populate only a fraction of the whole beam, resulting in a small measured cross section. The higher yield of signal for WF_5^- indicates that the vertical detachment energy for WF_5^- should be lower than the corresponding energy in HfF_5^-. This conclusion is also supported by calculations that predict the vertical detachment energies of WF_5^- and HfF_5^- to be 3.9 eV (31455 cm^{-1}) and 9.5 eV (76622 cm^{-1}), respectively [36]. A large molecular anion such as WF_5^- will probably support a rather large spectrum of ro-vibrationaly excited states which will be populated in the sputter source. Therefore we will not observe a zero cross section beneath the steep rise of the ground state cross section, but rather a slowly growing yield of signal as more and more excited-state photodetachment channels open. The fact that the neutral HfF_5 is unstable further com-

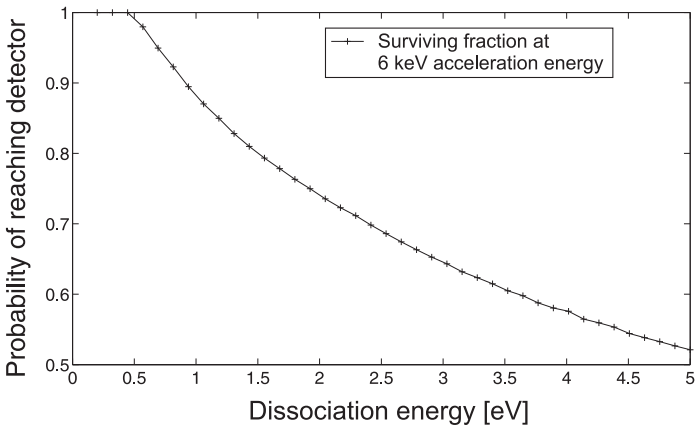

Figure 7.14: The probability for a dissociated HfF_5, i.e. a HfF_4 neutral to reach the detector as a function of dissociation energy. The simulation assume an isotropic angular distribution of the recoil in a cylindrical geometry. The result shown is valid for a 6 keV acceleration energy of the ion beam.

plicates the matter. Depending on how big the dissociation energy is when the HfF_5^- goes to HfF_4^-, some fraction of the photodetached ions could be lost. Due to the recoil effect they will drift out of the interaction region and will not make it through the second 3 mm aperture. A rough simulation (Fig. 7.14) shows that a dissociation energy of 1 eV will cause a loss of approximately 10 % from the signal. This will not significantly change the result of the experiment.

Unfortunately we could not reach the predicted ground-state detachment energy for WF_5^- due to the transmission properties of the conducting coating on the glass plate in the detector. The In_2O_3:Sn coating has a sharp cutoff in transmission around 350 nm and a replacement coating with suitable optical properties has not yet been found.

7.3.4 Paper X : Improved method for determination of the suppression of isobars in a gas-filled RF quadrupole ion guide.

In paper **X** we present a study of the magnitude of isobar suppression attainable in a gas filled radio frequency quadrupole. The experiment was performed at Oak Ridge National Lab in Tennessee. A Co sample was used to produce a beam of Co^--ions which was guided through the RF quadrupole. The gas filled quadrupole ion guide and the experimental setup is described in section 6.5 and in references [78] and [101]. The transit time for the beam through the ion guide was on the order of ms. Earlier measurements were made by extracting the depletion of the ion beam from the ion current measured with a Faraday cup at the end of the beam line [77]. This cup has a noise

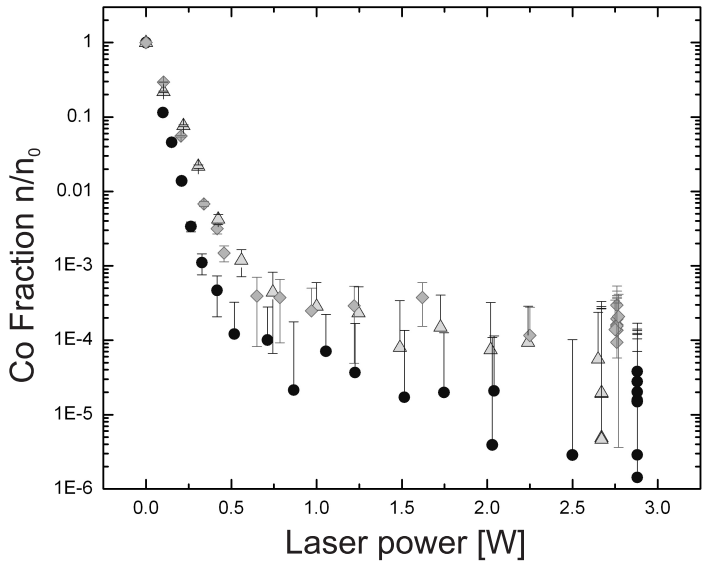

Figure 7.15: The ratio of depletion of the Co^-beam as a function of laser power. Squares and triangles are data where a suppression laser rate of 10 kHz was used. 20 kHz was used for the filled circles.

level of 10^{-13}A and when this was reached no further useful data could be recorded. The new detection scheme uses a neutral particle counting detector with a very low sensitivity limit. Meaningful results could easily be acquired with a signal rate of 1 Hz, corresponding to 10^{-19} A. The degree of depletion of the Co^- beam was measured as functions of laser power and buffer gas pressure in the ion guide. The result is shown in figures 7.15 and 7.16. The part of the data between a suppression laser power of 0 to approximatively 0.7 W follows an exponential decrease, but at higher laser power a much smaller decrease of the ion beam is seen. The reason for this "baseline" is unclear. The most probable explanation is contaminants of a higher EA such as the high energy tail of $^{58}Ni^-$ or isobars such as Al_2O^-. During the experiment the cathode was changed from a mixed Ni/Co -sample to a pure Co sample with no significant change in the baseline, which suggests that a high energy tail of $^{58}Ni^-$ may not be the source of the photodetachment signal. The Co-sample has been exposed to air for a long time and will hence contain some oxides. There could also be some aluminum present in the cathode material, the sample holder material, or in the source interior. The electron affinity of Al_2O is 4.23 eV, much higher than the energy of the applied radiation which is 1.165 eV . However, if Al_2O is the contamination, a fraction of the molecules can leave the ion source in excited states, which may explain the weak but visible power dependance of the signal. For the moment, however, the source of the photodetachment- and collision-signal below 0.7 W remains unclear.

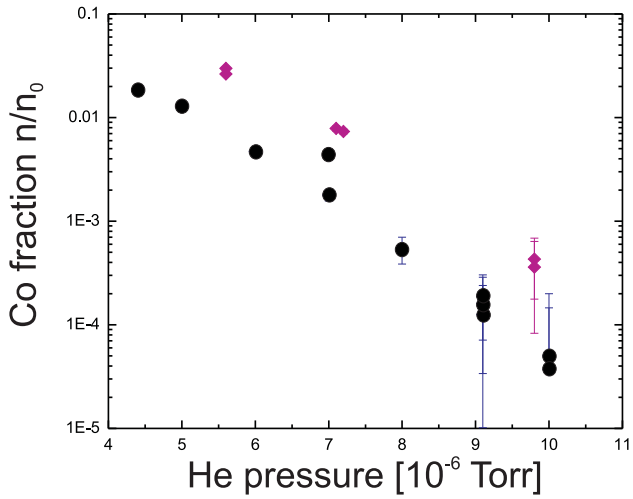

Figure 7.16: The maximum suppression as a function of relative pressure in the ion guide. As above the filled circles represent a 20 kHz repetition rate on the suppressing laser. 10 kHz was used for the data represented by the filled squares.

The pressure dependence, in contrast, follows a pure exponential behavior. There is of course no reason to raise the pressure infinitely since raising the pressure involves a trade off between increased suppression and beam transmission through the ion guide. Note that the measured pressure is not the pressure in the actual ion guide but a relative measurement by an ion gauge inside the vacuum vessel containing the enclosed ion guide. It is also interesting to note that the maximum suppression changes with the repetition frequency of the laser, even though the power is constant. The reason for this is presently also unclear, but might just be an effect of the laser power measurement. Since the laser power measurement equipment is meant to be used for CW laser there might be a frequency compensating factor that has been overlooked in the data analysis. One other possible explanation to both the ”baseline” and the frequency dependance is that there are two distinct fractions in the Co^- -beam passing through the ion cooler, one of which is much less exposed to the laser light due to its trajectory or speed.

Nevertheless, the suppression of 99.995% of the Co^- beam is a powerful depletion. A measurement under identical conditions was made on $^{58}Ni^-$ and showed only a 20% decrease of the ion beam. Some effect on Ni was expected since the energy of the laser light is slightly above the Ni^- p- wave photodetachment threshold. The fact that four orders of depletion was reached by just 0.5 W of laser power with only a minor effect on the $^{58}Ni^-$ makes this technique very promising for implementation into mass

spectrometric systems.

8

Conclusion and Outlook

The work presented this thesis has been on three different aspects of negative ions. The first part has focused on the structure of negative ions. The experiments have added to the general fundamental knowledge of the atomic negative ions. There is still insufficient knowledge of many ions, as shown by the indication of an unknown state in tungsten, which would be a future target for both experiment and theory, and by the detection and determination of the $^2S_{1/2}$ state in Pt^- at an energy almost 1000 cm^{-1}away from the predicted position. The experiment on Ce^- showed several features that could not be uniquely identified. To do so one might have to use a laser depletion method that removes the population of excited states in the negative ion so that the initial state of the transitions can be absolutely determined. This could, for example, be easily and effectively done in a gas filled RF quadrupole ion guide. Alternatively the electric-field detachment technique used by the group of Kellerbauer to re-measure the excited state in osmium [118] first observed by Bilodeau *et al.* [53] could be applied on cerium to prove without doubt the existence of a weakly bound state with a parity opposite that of the ion ground state. If such a state, causing the resonance A in paper **III**, is bound with an energy too large for an electric-field detaching scheme to be effective, the radiation from a CO_2 laser could be used as the detaching mechanism when searching for the energy of the transition from the ground state. In addition to cerium, many others of the weakly bound Lanthanide ions are still not experimentally verified and fully mapped. It would also be highly interesting to perform a high-resolution determination of the EA of H, the only element in which this quality more accurate known theoretically then experimentally.

The second part of this thesis focused on the dynamics of negative ions. A novel scheme, including the use of a storage ring and a laser probing tool is used to measure the very long lifetimes of metastable excited states in three different ions. Due to the selection rules for dipole transitions the lifetimes of these states are on the order of seconds or milliseconds and therefore too long to be measured in a linear accelerator. They decay by multi-pole processes to the ion ground state in contrast to the lifetimes of auto detaching metastable states in negative ions measured by Pedersen *et al.* [119, 120]. By

storing the ions a sufficiently long time in a storage ring we managed to probe the excited state during a time interval that allowed us to fit a double exponential function to the data. These studies can hopefully continue once the electrostatic double ring DESIREE in Stockholm begins to operate [121].

The last part of the work was dedicated to the development of a laser based technique to suppress isobars and neighboring isotopes that could contaminate a mass-selected beam. The selective detection of specific isotopes was demonstrated on both sulfur, where the isotopes were two mass units apart, and on carbon, where the mass difference between the isotopes was 1 u. The experiments showed that we could suppress the detection the unwanted isotope by as much as 98%.

In paper IX a search for the opening of the ground state photodetachment channel for both WF_5^- and HfF_5^- was performed. The hope is that the tungsten fluoride photodetachment channel would open earlier than the corresponding channel on the hafnium fluoride and thus allow for a laser suppression of the unwanted WF_5^- molecule. The result shows no definitive sign of such an opening and the signal is interpreted as photodetachment from a small fraction of excited state molecules. The search towards higher photon energies was stopped at 3.5 eV due to transmission losses in the glass plate in the neutral particle detector. Calculations suggest that the photodetachment threshold for WF_5^- lies just below 4 eV so a continued investigation using an optically suitable conducting coating, if possible, or a transition to a crossed beam geometry would be interesting.

The possibilities for a large suppression of ion beam contaminants by laser light in combination with a gas filled RF quadrupole ion guide was investigated on a Co^- beam at Oak Ridge National Lab. A suppression of over four orders of magnitude is a substantial reduction that may help in many future experiments. As mentioned earlier, in AMS the alternative method of energy straggling in matter is most suitable for lighter ions, and even then the suppression in the $^{36}Ca/^{36}S$ case is only just over two orders of magnitude [83]. This means that the method demonstrated here could be of great use even for lighter ions. A particulary interesting application would be as a suppressor to remove $^{12}CH_2^-$ and $^{13}CH^-$ from a beam of $^{14}C^-$. The problem of isobaric molecules gets worse as the acceleration voltages decrease in the new generations of AMS machines [122]. This laser detachment scheme could help remove these impurities from the beam. Moreover, after re-acceleration from the ion-cooler the high energy sputter tail, that could cause some $^{13}C^-$ to contaminate the $^{14}C^-$ beam, will be completely removed. There are many other isobaric pairs where this scheme could be used (see table 5.1) and even if the contaminating atomic ion does have a higher EA than the trace isotope in question, there might exist a molecule where this is not the case. An example is the ultra trace isotope ^{60}Fe which has an electron affinity of 0.151(3) eV. The contam-

inant, ^{60}Ni, does have a much higher EA (1.157 eV) but their respective hydrides have the opposite relation, with detachment energies of 0.934 and 0.481 eV for FeH^- and NiH^-, respectively. Thus, laser suppression in a gas filled radio frequency ion guide could be feasible if one used the hydride as the injected particle.

Hopefully, the work of this thesis has revealed a few interesting and useful facts about negative ions. In particular I hope that some of the experiments presented here will be part of the body of work that will push the limit of mass spectrometry into the future.

Acknowledgements

The crooked path leading to this thesis has not been a lonely one. Many friends and kind people have been accompanying me along the journey, some only for a short time and others for most of the way. I wish to thank them for showing me the proper directions, brightening the road and helping me to reach the destination in many different ways. In particular I would like to mention:

My supervisor Professor Dag Hanstorp, who is one of the most understanding and positive persons I ever met. No matter how much he has to do, he always has time to give good advice. For every problem facing me, he has given a suggestion of how to solve it or shown me a way to look at it, not as a problem but as something good. He has a deep and intuitive knowledge of physics and a wonderful ability to transfer that knowledge in an understandable and interesting way. I would like to thank him for his faith in me and for his support during hard times. My examiner Professor Eleanor Campbell, who actually, probably unknowingly, turned me on to this subject. It was during an assignment in one of her atomic physics courses that I first became acquainted with negative ions. It has been an honor to work for such a skilled and eminent scientist. I would also like to thank her for giving me the opportunity to experience the Burns night including haggis and poetry reading. The honorary doctor Professor David Pegg, who has taught me much about physics in general and negative ions in particular. His knowledge of the field is immense and his help has been a great asset in my work. I would like to thank him for helping out in the lab and with the writing of articles. Thank you also for everything I have learnt about football, Cornwall and many other un-physical topics, both on and off working hours. In the last year I was fortunate to be able to work with Professors Yuan Liu and Charles Havener, both at Oak Ridge National Lab. I would like to thank them for the invitation and for a rewarding cooperation. I would like to thank Professor Dan Gibson from Denison University, Granville Ohio for fruitful and enjoyable collaborations in Gothenburg, at CRYRING and ALS, and in Granville. I would like to thank him, as well as Professor Wesley Walter from the same university, for giving me and my family the opportunity to go to Granville. I also want to thank both of their families for taking such good care of us. The whole crew at the Manne Siegbahn Laboratory must be acknowledged for their work when reversing the ring for running negative ions and their help during the experiments. The atomic physics group at Stockholm University, especially Sven Mannervik and old and present PhD students Jonas Gurell, Peter Schef and Peter Lundin is thanked for the possibility of joining our forces for experiments at CRYRING, interesting discussions and nice company at conferences. The same must be said of the Molecular Physics group at Stockholm University, in particular Dr. Richard Thomas who proof-read this thesis and has traveled to Gothenburg on several occasions to help out with our work. Thank you. Much of the application studies presented in this thesis could not have been done without the aid of Professor Klaus Wendt and Christoph

Diehl from the University of Mainz. Thank you. Christoph is currently working on his PhD at the Max Planck Institute in Heidelberg. I wish him good luck. The negative ion group at the atomic physics department in Gothenburg is vital in the work presented here: I thank my room mate Lic. Anton Lindahl for really good co-working, inspiring discussions, clarifying explanations and pleasant company. Former room mates and PhD students Dr. Karin Fritioff and Dr. Joakim Sandström should both be acknowledged for their contributions, not only as co-authoring scientists but also for teaching me the basics and getting me started as a PhD student. New members of the group, Dr. Peter Klason and future doctor Johan Rohlén have contributed valuable work in the last six months. Other members and former members of the atomic physics department are also acknowledged for nice comradeship and helping out whenever needed: Gerry Collins, Klavs Hansen, Martin Hedén, Mikael Kjellberg, Ingvar Lindgren, Martin Jönsson, Niklas Olofsson, Sten Salomonson, Martin Svenningsson, Johannes Svensson, Erika Sundin, Anne-Marie Pendrill, Vladimir Popok, Saša Vučković. Special thanks go to Daniel Hedendahl and Anders Börjesson for being my friends all the way from the start in 1998 - both in physics, music and everyday life. The department and in particular the atomic physics lab would not be able to run without the knowledge and skills of Heinrich Riedel, Jan-Åke Wiman and Mats Rostedt. Nor would the department function if Rose Marie Wikström and Bea Augustsson were not here to take care of us.

Above all I would like to thank the love of my life, Cecilia, for her wholehearted support and my sons Tage and Ruben for being endless sources of joy. Finally I would like to thank my parents who have always supported me, whatever I have decided to do.

Bibliography

[1] Thomson, J. J. *proceedings of the royal soc.* **A 89**, 1–20 (1913).

[2] Massey, H. S. W. *Negative ions*. Cambridge University Press, London, 1 edition, (1938).

[3] Wildt, R. *Astrophys. J.* **93**, 47–51 (1941).

[4] Chandrasekhar, S. *Reviews of modern physics* **16**(3,4), 301–306 (1944).

[5] Fite, W. L. *Phys. Rev.* **89**(2), 411–415 Jan (1953).

[6] Branscomb, L. M. and Fite, W. L. *Phys. Rev.* **93**, 47–45 (1954).

[7] Branscomb, L. M. and Smith, S. J. *Phys. Rev.* **98**, 1028–1034 (1955).

[8] Massey, H. S. W. *Negative Ions*. Cambridge University Press, London, (1976).

[9] Smirnov, B. M. *High Temperature* **3**(5), 716 (1965).

[10] Lineberger, W. C. and Woodward, B. W. *Phys. Rev. Lett.* **25**(7), 424–427 Aug (1970).

[11] Hotop, H., Patterson, T. A., and Lineberg, W. C. *Bulletin Of The American Physical Society* **17**(1), 150 (1972).

[12] Patterson, T. A. ., Hotop, H., and Lineberger, W. C. *Bulletin Of The American Physical Society* **17**(11), 1128 (1972).

[13] Hotop, H., Bennett, R. A., and Lineberger, W. C. *Journal Of Chemical Physics* **58**(6), 2373–2378 (1973).

[14] Hotop, H. and Lineberger, W. C. *Journal Of Chemical Physics* **58**(6), 2379–2387 (1973).

[15] Hotop, H. and Lineberger, W. C. *Journal of Physical and Chemical Reference Data* **4**(3), 539–576 (1975).

[16] Andersen, T., Haugen, H. K., and Hotop, H. *J Phys. Chem. Ref. Data* **28**, 1511–1533 (1999).

[17] Andersen, T. *Physics Reports* **394**(4-5), 157 (2004).

[18] Pegg, D. J. *Reports on Progress in Physics* **67**(6), 857 (2004).

[19] Buckman, S. J. and Clark, C. W. *Rev. o. Mod. Phys.* **66**, 535–655 (1994).

[20] Pegg, D. J., Thompson, J. S., Compton, R. N., and Alton, G. D. *Phys. Rev. Lett.* **59**(20), 2267–2270 Nov (1987).

[21] Fischer, C. F., Lagowski, J. B., and Vosko, S. H. *Phys. Rev. Lett.* **59**(20), 2263–2266 Nov (1987).

[22] Walter, C. W. and Peterson, J. R. *Physical Review Letters* **68**(15), 2281–2284 APR 13 (1992).

[23] Nadeau, M.-J., Zhao, X.-L., Garwan, M. A., and Litherland, A. E. *Phys. Rev. A* **46**, R3588–R3590.

[24] Haugen, H. K., Andersen, L. H., Andersen, T., Balling, P., Hertel, N., Hvelplund, P., and Möller, S. P. *Phys. Rev. A* **46**, R1–R4 (1992).

[25] Petrunin, V. V., Andersen, H. H., Balling, P., and Andersen, T. *Phys. Rev. Lett.* **76**, 744–747 (1996).

[26] Amemiya, H. and Nakamura, Y. *Journal Of Geomagnetism And Geoelectricity* **45**(3), 219–230 (1993).

[27] Petrie, S. and Bohme, D. K. *Mass spectrometry reviews* **26**(2), 258–80 (2007).

[28] McCarthy, M. C., Gottlieb, C. A., Gupta, H., and Thaddeus, P. *Astrophysical Journal* **652**(2, Part 2), –141 DEC 1 (2006).

[29] Brunken, S., Gupta, H., Gottlieb, C. A., McCarthy, M. C., and Thaddeus, P. *Astrophysical Journal* **664**(1, Part 2), –43 JUL 20 (2007).

[30] Cernicharo, J., Guelin, M., Agundez, M., McCarthy, M. C., and Thaddeus, P. *Astrophysical Journal Letters* **688**, L83–L86 (2008).

[31] Economou, D. *Applied Surface Science* **253**(16), 6672 (2007).

[32] Mason, N. J. and Skalny, J. D. *19th Europhysics Conference on the Atomic and Molecular Physics of Ionized Gases, Granada, Spain* (2008).

[33] PORTIER, S. *International Journal of Mass Spectrometry* **263**(2-3), 113 (2007).

[34] Seki, M. *Nuclear Fusion* **47**(10), –489 OCT (2007). 21st IAEA Fusion Energy Conference, Chengdu, Peoples R China, OCT 16-21, 2006.

[35] O'Malley, S. M. and Beck, D. R. *Physical Review A (Atomic, Molecular, and Optical Physics)* **74**(4), 042509 (2006).

[36] Hongshan, C. Private comunication, December (2008).

[37] Drake, G. W. F., Cassar, M. M., and Nistor, R. A. *Phys. Rev. A* **65**(5), 054501 (2002).

[38] Walton, D. S., Peart, B., and Dolder, K. T. *J. Phys. B: Atom. molec. Phys.* **4**, 1343–1348 (1971).

[39] Chang, K. H., McKeown, R. D., Milner, R. G., and Labrenz, J. *Phys. Rev. A* **35**(9), 3949–3951 May (1987).

[40] H. Gnauser, A. D. and Cederbaum, L. S. *Journal of chemical physics* **117**(15), 7002–7009 (2002).

[41] Pedersen, H. B., Djurić, N., Jensen, M. J., Kella, D., Safvan, C. P., Vejby-Christensen, L., and Andersen, L. H. *Phys. Rev. Lett.* **81**(24), 5302–5305 Dec (1998).

[42] Farley, J. W. *Phys. Rev. A* **40**, 6286–6292 (1989).

[43] Wigner, E. P. *Phys. Rev.* **73**, 1002 (1948).

[44] O'Malley, T. F. *Phys. Rev.* **137**(6A), –1668 Mar (1965).

[45] Smith, Stephen J. and Burch, David S. *Phys. Rev. Lett.* **2**, 165–166 (1959).

[46] Prasad, M. S. and Sen, K. D. *The Journal of Chemical Physics* **95**, 1421 (1991).

[47] Radojević, V., Kelly, H. P., and Johnson, W. R. *Phys. Rev. A* **35**(5), 2117–2121 Mar (1987).

[48] Shannon, R. D. *Acta Crystallographica Section A* **32**, 751–767 (1976).

[49] Eder, R., Pen, H. F., and Sawatzky, G. A. *Phys. Rev. B* **56**, 10115 (1997).

[50] H. J. Kaiser, and E. Heinicke, and R. Rackwitz and D. Feldmann . *Zeitschrift für Physik A Hadrons and Nuclei* **270**, 259–265 (1974).

[51] Scheer, M., Haugen, H. K., and Beck, D. R. *Phys. Rev. Lett.* **79**(21), 4104–4107 Nov (1997).

[52] Scheer, M., Bilodeau, R. C., and Haugen, H. K. *J. Phys. B* **31**, –11 (1998).

[53] Bilodeau, R. C. and Haugen, H. K. *Phys. Rev. Lett.* **85**, 534–537 (2000).

[54] Branscomb, L. M. and Smith, S. J. *Phys. Rev.* **98**(4), 1127–1128 May (1955).

[55] Haeffler, G., Ljungblad, U., Kiyan, I. Y., and Hanstorp, D. *Zeitschrift Fur Physik D-Atoms Molecules And Clusters* **42**(4), 263–266 DEC (1997).

[56] Covington, A. M., Calabrese, D., Williams, W. W., Thompson, J. S., and Kvale, T. J. *Phys. Rev. A* **56**(6), 4746–4754 Dec (1997).

[57] Hanstorp, D., Bengtsson, C., and Larson, D. J. *Phys. Rev. A* **40**(2), 670–675 Jul (1989).

[58] Williams, W. W., Carpenter, D. L., Covington, A. M., Koepnick, M. C., Calabrese, D., and Thompson, J. S. *Journal Of Physics B-Atomic Molecular And Optical Physics* **31**(8), –341 (1998).

[59] Hanstorp, D. *Nucl. Instr. and Meth. B* **100**, 165 (1995).

[60] Kaufman, S. L. *Optics Communications* **17**(3), 309–312 (1976).

[61] Juncar, P., Bingham, C. R., Bounds, J. A., Pegg, D. J., Carter, H. K., Mlekodaj, R. L., and Cole, J. D. *Phys. Rev. Lett.* **54**, 11–13 (1985).

[62] Valli, C., Blondel, C., and Delsart, C. *Phys. Rev. A* **59**(5), 3809–3815 May (1999).

[63] Anderson, E. C., Libby, W. F., Weinhouse, S., Reid, A. F., Kirshenbaum, A. D., and Grosse, A. V. *Phys. Rev.* **72**, 931–936 (1947).

[64] Currie, L. A. *Journal of Research of the National Institute of Standards and Technology* **109**(2), 185–217 (2004).

[65] Nelson, D. E., Korteling, R. G., and Stott, W. R. *Science* **198**, 507–508 (1977).

[66] Bennet, C. L., Beukens, R. P., Clover, M. R., and Gove, H. E. *science* **198**, 508–510 (1977).

[67] Welten, K. C., Hillegonds, D. J., Masarik, J., and Nishiizumi, K. *Nuclear Instruments and Methods in Physics Research Section B: Beam Interactions with Materials and Atoms* **259**, 653–662 (2007).

[68] Reedy, R. C. *Nuclear Instruments and Methods in Physics Research Section B: Beam Interactions with Materials and Atoms* **223-224**, 587–590 (2004).

[69] Hou, X. and Roos, P. *Analytica Chimica Acta* **608**(2), 105–139 (2008).

[70] Steinhausen, C., Gerisch, P., Heisinger, B., Hohl, C., Kislinger, G., Korschinek, G., Niedermayer, M., Nolte, E., Dumitru, M., Alvarez-Brockmann, M., Schneider, M., and Ittel, T. H. *Nuclear Instruments and Methods in Physics Research Section B: Beam Interactions with Materials and Atoms* **113**, 479–483 (1996).

[71] Wendt, K. and Trautmann, N. *International Journal of Mass Spectrometry* **242**, 161–168 (2005).

[72] Hellborg, R. and Skog, G. *Mass Spectrometry Reviews* **27**, 398–427 (2008).

[73] Kutschera, W. *International Journal of Mass spectrometry* **242**, 145–160 (2005).

[74] Ruff, M., Wacker, L., Gaeggeler, H. W., Suter, M., Synal, H. A., and Szidat, S. *Radiocarbon* **49**, 307–314 (2007).

[75] Berkovits, D., Boaretto, E., Hollos, G., Kutschera, W., Naaman, R., Paul, M., and Vager, Z. *Nuclear Instruments and Methods in Physics Research Section A: Accelerators, Spectrometers, Detectors and Associated Equipment* **281**(3), 663–666 (1989).

[76] Berkovits, D., Boaretto, E., Hollos, G., Kutschera, W., Naaman, R., Paul, M., and Vager, Z. *Nuclear Instruments and Methods in Physics Research Section B Beam Interactions with Materials and Atoms* **52**(3-4), 378–383 (1990).

[77] Liu, Y., Beene, J. R., Havener, C. C., and Liang, J. F. *Applied Physics Letters* **87**(11) (2005).

[78] Liu, Y., Liang, J. F., Alton, G. D., Beene, J. R., Zhou, Z., and Wollnik, H. *Nuclear Instruments & Methods In Physics Research Section B-Beam Interactions With Materials And Atoms* **187**(1), 117–131 (2002).

[79] Fields, B. D., Hochmuth, K. A., and Ellis, J. *Astrophysical Journal* **621**(2, Part 1), 902–907 (2005).

[80] Knie, K., Korschinek, G., Faestermann, T., Dorfi, E. A., Rugel, G., and Wallner, A. *Phys. Rev. Lett.* **93**(17), 171103 (2004).

[81] Fitoussi, C., Raisbeck, G. M., Knie, K., Korschinek, G., Faestermann, T., Goriely, S., Lunney, D., Poutivtsev, M., Rugel, G., Waelbroeck, C., and Wallner, A. *Physical Review Letters* **101**(12), 121101 (2008).

[82] Winkler, S. *Nuclear Instruments and Methods in Physics Research Section B Beam Interactions with Materials and Atoms* **259**(1), 256 (2007).

[83] Klein, M. G., Gottdang, A., Mous, D. J. W., Bourlés, D. L., Arnold, M., Hamelin, B., Aumaître, G., Braucher, R., Merchel, S., and Chauvet, F. *Nuclear Instruments and Methods in Physics Research Section B: Beam Interactions with Materials and Atoms* **266**(8), 1828–1832 (2008).

[84] Vockenhuber, C. *Nuclear Instruments and Methods in Physics Research Section B Beam Interactions with Materials and Atoms* **223-224**, 823 (2004).

[85] Krohn, V. *Journal Of Applied Physics* **33**(12), 3523 (1962).

[86] Middleton, R. and Adams, C. T. *Nuclear Instruments and Methods* **118**(2), 329–336 (1974).

[87] Middleton, R. http://130.199.216.18/cookbook/. A Negative-Ion Cookbook.

[88] Alton, G. D. and Jones, C. M. *Nuclear Instruments and Methods in Physics Research Section A: Accelerators, Spectrometers, Detectors and Associated Equipment* **244**(1-2), 170–175 (1986).

[89] Alton, G. D., Mori, Y., Takagi, A., Ueno, A., and Fukumoto, S. *Nuclear Instruments and Methods in Physics Research Section B: Beam Interactions with Materials and Atoms* **40-41**(Part 2), 1008–1013 (1989).

[90] Yu, M. L. *Phys. Rev. Lett.* **40**, 574–577 (1978).

[91] Balling, P., Andersen, H. H., Brodie, C. A., Pedersen, U. V., Petrunin, V. V., Raarup, M. K., Steiner, P., and Andersen, T. *Phys. Rev. A* **61**(2), 022702 (2000).

[92] Tang, C. Y., Harris, P. G., Mohagheghi, A. H., Bryant, H. C., Quick, C. R., Donahue, J. B., Reeder, R. A., Cohen, S., Smith, W. W., and Stewart, J. E. *Phys. Rev. A* **39**, 6068–6071 (1989).

[93] Quick, C. R., Donahue, J. B., Cohen, S., Bryant, H. C., Tang, C. Y., Harris, P., Mohagheghi, A. H., Reeder, R. A., Sharifian, H., Toutounchi, H., and Smith, W. W. *Nuclear Instruments & Methods In Physics Research Section B-Beam Interactions With Materials And Atoms* **56-7**, 205–210 (1991).

[94] Tang, C. L. and Cheng, L. K. *Fundamentals of Optical Parametric Processes and Oscillations*. Harwood Academic Publishers, (1996). ISBN 3-7186-5818-6.

[95] Hanstorp, D. *Meas.Sci.Technol* **3**, 523–527 (1992).

[96] Fritioff, K., Sandström, J., Andersson, P., Hanstorp, D., Hellberg, F., Thomas, R., Geppert, W., Larsson, M., Österdahl, F., Collins, G. F., Pegg, D. J., Danared, H., Källberg, A., and Gibson, N. D. *Phys. Rev. A* **69**, 042707 (2004).

[97] Fritioff, K. *Journal of Physics B Atomic Molecular and Optical Physics* **37**(11), 2241 (2004).

[98] Hartman, H., Rostohar, D., Derkatch, A., Lundin, P., Schef, P., Johansson, S., Lundberg, H., Mannervik, S., Norlin, L. O., and Royen, P. *J. Phys. B* **36**, –197 (2003).

[99] Hartman, H., Gurell, J., Lundin, P., Schef, P., Hibbert, A., Lundberg, H., Mannervik, S., Norlin, L. O., and Royen, P. *Astronomy & Astrophysics* **480**(2), 575–580 (2008).

[100] Simonsson, A. *Beam Dynamics and Injection in CRYRING*. PhD thesis, Manne Siegbahn Institute of Physics, Royal Institute of Technology, (1991).

[101] LIU, Y. *Nuclear Instruments and Methods in Physics Research Section B Beam Interactions with Materials and Atoms* **255**(2), 416 (2007).

[102] Feldmann, D. *Zeitschrift Fur Physik A-Hadrons And Nuclei* **277**(1), 19–25 (1976).

[103] Slater, J. and Lineberger, W. C. *Phys. Rev. A* **15**(6), 2277–2282 (1977).

[104] Feigerle, C. S., Corderman, R. R., Bobashev, S. V., and Lineberger, W. C. *The Journal of Chemical Physics* **74**(3), 1580–1598 (1981).

[105] Bengali, A. A., Casey, S. M., Cheng, C. L., Dick, J. P., Fenn, P. T., Villalta, P. W., and Leopold, D. G. *Journal of the American Chemical Society* **114**(13), 5257–5268 (1992).

[106] Davis, V. T., Thompson, J., and Covington, A. *Nuclear Instruments & Methods In Physics Research Section B-Beam Interactions With Materials And Atoms* **241**, 118–124 (2005).

[107] Davis, V. T. and Thompson, J. *Phys. Rev . Lett.* **88**, 073003 (2002).

[108] Saitoh, Y., Yotsombat, B., Mizuhashi, K., and Tajima, S. *The 8th interntaional conference on ion sources* **71**(2), 955–957 (2000).

[109] Nadeau, M.-J., Litherland, A. E., Garwan, M. A., and Zhao, X.-L. *Nuclear Instruments and Methods in Physics Research Section B: Beam Interactions with Materials and Atoms* **92**, 265 – 269 (1994).

[110] Cao, X. *Physical Review A* **69**(4), 042508 (2004).

[111] Zollweg, R. J. *The Journal of Chemical Physics* **50**(10), 4251–4261 (1969).

[112] Thøgersen, J., Scheer, M., Steele, L. D., Haugen, H. K., and Wijesundera, W. P. *Phys. Rev. Lett.* **76**(16), 2870–2873 (1996).

[113] Bilodeau, R., Scheer, M., Haugen, H., and Brooks, R. *Physical Review A* **61**, art. no.–012505 (2000).

[114] Mannervik, S., Brostrom, L., Lidberg, J., Norlin, L., and Royen, P. *Hyperfine Interactions* **108**, 291–304 (1997).

[115] Lidberg, J., Al-Khalili, A., Norlin, L. O., Royen, P., Tordoir, X., and Mannervik, S. *Nucl. Instr. and Meth. B* **152**, 157–170 (1999).

[116] O'Malley, S. M. and Beck, D. R. *J. Phys. B* **36**(4301), 4301 (2003).

[117] Diehl, C. Master's thesis, February (2008).

[118] Warring, U., Amoretti, M., Canali, C., Fischer, A., Heyne, R., Meier, J. O., Morhard, C., and Kellerbauer, A. *Phys. Rev. Lett.* **102** (2009).

[119] Pedersen, U. V., Hyde, M., Møller, S. P., and Andersen, T. *Phys. Rev. A* **64**, 012503 (2001).

[120] Pedersen, U. V., Svendsen, A., Blæsild, P., and Andersen, T. *J. Phys. B* **35**, 2811 (2002).

[121] Danared, H., Liljeby, L., Andler, G., Bagge, L., Blom, M., Kallberg, A., Leontein, S., Lofgren, P., Paal, A., Rensfelt, K. G., Simonsson, A., Schmidt, H. T., Cederquist, H., Larsson, M., Rosen, S., and Schmidt, K. In *Beam Cooling and Related Topics,* Nagaitsev, S. and Pasquinelli, R. J., editors, volume 821 of *AIP Conference Proceedings*, 465–472. Amer Inst Physics, (2006). International Workshop on Beam Cooling and Related Topics (COOL05), Galena, IL, SEP 18-23, 2005.

[122] Suter, M. *Nuclear Instruments and Methods in Physics Research Section B Beam Interactions with Materials and Atoms* **223-224**, 139 (2004).

Paper I

Paper II

Paper III

Paper IV

Paper V

Paper VI

Paper VII

Paper VIII

Paper IX

Paper X